Proceedings of the Institution of Mechanical Engineers, Part C: Journal of Mechanical Engineering Science,
Vol 232, Issue9, 2018, pp. 1707-1733
DOI:10.1177/0954406217707983

Heat dissipation from a stationary brake disc

Part 1: Analytical Modelling and Experimental Investigations

*Kevin Stevens and Marko Tirovic**
Cranfield University, Cranfield, MK43 0AL, UK

**Corresponding author: m.tirovic@cranfield.ac.uk*

Abstract:

The main aim of the research is to support the development of the commercial vehicle (CV) electric parking brake (EPB). Though nowadays widely used on passenger cars, EPB applications on CVs present completely different challenges. With the brake mass, thermal capacity and required clamp forces an order of magnitude higher, safe parking demands much more attention. In the first instance, the priority is placed upon predicting heat dissipation from the brake disc only.

The research is presented in two parts; part one (presented here) focuses on analytical modelling and experimental verification of predicted disc temperatures over long cooling periods, with part two investigating the air flow, velocities and convective heat transfer coefficients using Computational Fluid Dynamics modelling, also followed by experimental validations.

To begin the analytical analysis, a study was conducted into the variance in mean local convective heat transfer coefficients over a simplified brake disc friction surface, by investigating typical dimensionless air properties. A non-linear equation was derived for the average surface convective heat transfer coefficient (h_{conv}) variability with temperature drop for the entire cooling phase. Starting from fundamental principles, first order differential equations were developed to predict the bulk disc temperature. By including variation of the convective and radiative heat dissipation throughout the cooling period, a good correlation was achieved with measured values, to within 10%.

Experiments were conducted on a specifically designed Thermal Rig which uses 15 kW induction heater to heat the disc. Numerous experiments proved the results are very repeatable, throughout the cooling period. It was established, for the grey cast iron brake disc with a fully oxidised surface, the emissivity

value are practically constant at ε = 0.92. Although the research is being conducted on a brake disc, the results have generic application to any disc geometry, whatever the application.

Keywords: Stationary Disc; Brake Disc; Convective Cooling; Emissivity; Heat dissipation.

Nomenclature:

Symbol	**Description**
A	Surface area
C_p	Specific heat capacity
D	Diameter
E	Energy
Fo	Fourier Number
g	Gravitational acceleration (9.81m/s^2)
Gr	Grashof number
h	Bulk heat transfer coefficient
k	Thermal conductivity
l	Length
L	Characteristic length
m	Mass
Nu	Nusselt number
Pr	Prandtl number
p	Pressure
Q	Power
r	Radius
Ra	Rayleigh number
Re	Reynolds number
t	Time
T	Temperature
V	Speed (velocity)
α	Thermal diffusivity
ε	Emissivity
ζ	Coefficient of thermal expansion

μ	Dynamic viscosity
ν	Kinematic viscosity
ρ	Density
σ	Stefan-Boltzmann constant (5.67037 E-8 $Wm^{-2}K^{-4}$)
σ	Standard deviation
v	Molecular diffusivity of momentum

Subscripts

arc	Arc
avg	Average
$cond$	Conduction/Conductive
$conv$	Convection/Convective
c	Carrier (wheel carrier)
cr	Critical
d	Disc
D	Diameter
i	Inner
int	Interface
m	Mean local value
o	Outer
rad	Radiation/Radiative
rec	Rectangle
$surf$	Surface
$total$	Total
w	Wall
∞	Ambient

Abbreviations

CFD	Computational Fluid Dynamics
CV	Commercial Vehicle
EPB	Electric Parking Brake
FE	Finite Element (Method)
HTC	Heat Transfer Coefficient
ID	Inner Diameter
OD	Outer Diameter

1. Introduction

So far, there has not been significant published research into heat dissipation from a stationary disc as a geometric shape. Similarly, there is not much published work on stationary brake disc cooling. Traditionally, this was considered to be a relatively specific problem, which does not attract attention due to relative design robustness to such a duty. However, recent trends in automotive development and braking system electrification require better understanding of brake thermal aspects in stationary conditions. No doubt that this knowledge will improve temperature predictions in various driving duties too, which has been traditionally researched primarily for moving vehicles, as disc/pad interface brake temperatures have crucial influence on the coefficient of friction (hence vehicle deceleration) and pad wear. It should be noted that stationary brake cooling is particularly important for city buses, as the vehicles spend considerable service time standing in bus stops, traffic lights etc.

The first step in achieving the above tasks is related to accurate prediction of brake disc temperatures. Once heat dissipation from the disc (on its own) is well understood and can be reliably predicted, the entire brake assembly, consisting of the brake disc, pads and caliper, can be analysed and corresponding models generated. This paper focuses on the former, the gathering of knowledge around commercial vehicle (CV) brake disc cooling in stationary conditions; the latter will be subject to future presentations. Authors' aim is to establish generic relationships and whenever possible enable others to use the research results, not limiting the findings to brake discs only. The research itself has two global objectives, to aid Electronic Parking Brake (EPB) development for CVs (where more complex models and instrumentation can be used), and for establishing a simplified, yet robust and sufficiently accurate thermal model for use on-board CVs for controlling EPBs.

To achieve the above, the authors are approaching the problem of heat dissipation from stationary discs by firstly using analytical methods. Calculated average heat transfer coefficients will then be entered in a developed numerical model to predict disc temperature throughout the cooling period. The results will be compared with temperatures measured on a specially developed Thermal Rig. This will conclude Part 1 of the Paper, as due to the volume of work not all findings can be presented in a single paper. In Part 2, detailed Computational Fluid Dynamics (CFD) analyses of stationary disc cooling will be

conducted, which will provide air flow information as well as local and average heat transfer coefficients. These results, complemented with pad and caliper thermal studies, will enable accurate temperature prediction of the entire brake assembly, which will be subject of future publications.

2. Research Motivation

Vehicle electrification has been driven by the need to reduce vehicle mass and enhance component functionality, aiming to increase payload and commercial vehicle availability, reduce fuel consumption (CO_2 emissions) and maintenance costs. This research supports the development of the EPB into CVs, as well as more extensive use of temperature sensitive electric and electronic components installed into brake calipers. These systems offer more compact, lighter components, lower consumption of compressed air, much reduced residual brake drag (when brakes are not applied), better on-board diagnostics and longer periods between servicing (by more uniform pad wear). Thermal aspects need to be considerably better understood, with heat dissipation from stationary brake being critical for component life, and most importantly vehicle safety when parking on a gradient with hot brakes. Disc and pad contraction, combined with caliper expansion during cooling in 'hot parking' conditions can cause vehicle rollaway, which particularly in the case of commercial vehicles can have very serious consequences.

The most important driving force in predicting disc brake temperature is certainly related to the introduction of Electric Parking Brake (EPB) in commercial vehicles. Already proven very successful in passenger cars, many advantages of EPB system can be implemented in CV. However, there are considerable challenges, primarily in regard to the order of magnitude higher clamp forces required and 'hot parking' performance. Commercial vehicle brake components are considerably larger, clamp forces much higher, and CV brakes have a much greater capacity for retaining thermal energy. Therefore, thermal aspects for electric parking of CV brakes require particular attention. Consequently, EPBs have not been fully implemented on CVs, where the spring actuated parking chamber design remains widely used. Initial electrification of the parking systems on CVs use electronic components to simply control the air release rather than being the actuating mechanism. Still, this approach offers some

advantages by reducing the number of air lines in the driver's cab, making the vehicle lighter and adding functionality.

The majority of recently published EPB research papers deal with the control system for the motor driving the EPB. For example, position and velocity monitoring by sensorless technology allows greater EPB actuation control [1] a fuzzy type numerical controller gives a faster motor response time compared to the standard PID controllers [2], whilst a fault detection system has been developed to give driver warnings if any of the commonly known EPB faults occur [3].

As for thermal aspects, friction couple cooling is a fundamental to any brake design. A variety of vane shapes have been used within the disc itself in attempts to optimise the air flow through the disc, generating superior convective cooling [4]. Convection has the greatest influence on the brake cooling characteristics during motion, becoming increasingly more so as the vehicle velocity increases due to the air pumping through the vanes faster [5]. Quality of the air flow is also important, not just the flow velocity. Regions of recirculation arise in the vanes, which reduces the convection process [5].

Computational Fluid Dynamics (CFD) modelling procedures have become an essential tool for both brake designers and researchers, providing better understanding of the flow field generated and to the convective heat transfer coefficients (h_{conv}). CFD has been successfully utilised to show that flow separation will occur on the leading edge surface for straight vane rotors, reducing h_{conv} values [6] compared to the trailing edge where a regular air flow is seen all along the vane.

Finite Element (FE) techniques can accurately predict brake temperature results [7], subject to correctly defined boundary conditions. The usefulness of FE analysis was displayed further with a coupled thermomechanical FE model estimating both the disc temperatures and thermal stresses caused during a heavy braking scenario, to evaluate when thermal cracks will appear in the rotors [8].

The work discussed above gives a summary to the research topics currently being investigated. They were all completed under dynamic situations and predominately on passenger cars, with very little work being published on static brake characteristics. However, thermal aspects, with regards to hot parking situations, are extremely important. A lack of vehicle motion causes the only air flow to occur from

natural convection, drastically reducing the cooling rate and vastly altering the heat flow patterns. Influences of heat flow from conduction, convection and radiation on the thermal contraction require considerable further studies.

Due to the smaller size and lower load requirements, passenger car EPBs have the luxury of over-clamping the brake without hindering the fatigue life of the brake caliper to counter the thermal contraction effects present in the brake disc and pads. Furthermore, a passenger vehicle EPB 're-energizes' the brake by applying a second stage clamp force, typically three minutes after the initial brake application.

CV brakes, on the other hand, have an order of magnitude greater clamp force and thermal capacity, allowing for a significantly larger quantity of thermal expansion. With additional thermal capacity, longer cooling times are expected whilst greater expansion instigates increased contraction during the parked brake cooling phase, generating uncertainty in brake performance. Hence the reason why EPBs, thus far, have not been fully integrated into CVs. Driven by the introduction of EPB to CVs, this paper investigates a variety of aspects and influencing parameters on static disc cooling. Ultimately, the aim is to establish accurate and reliable predictive models that shorten time to market.

3. Brake Disc Studied and Methodology Applied

Thus far, modelling heat transfer from stationary disc brakes has proven a more complex task compared to modelling dynamic scenarios. In the latter, symmetry about each vane channel and constant heat transfer coefficients (HTC) are valid assumptions to make with disc rotation and short braking times. However, because airflow is driven purely by natural convection and cooling times are much longer in stationary parking applications, heat transfer coefficients can no longer be assumed constant. To enable an accurate method of temperature prediction, the variability in convective heat transfer from the disc brake must be understood. To enable this knowledge to be acquired, the brake disc shown in Figure 1 was used for all modelling and testing purposes. The disc is made of grey cast iron, has a straight vane ventilated configuration and anti-coning geometry (see Figure 1). Further information on the brake disc used is presented in Table 1. The disc is of 'anti-coning' type, meaning the inboard disc friction face is

attached to the hat section. As the name suggests, the resultant thermal expansion does not cause much coning i.e. difference in axial displacement between disc OD and ID. By keeping friction surfaces flat, there is much less tendency for uneven pad wear and most importantly brake judder (low frequency vibration) with this disc type.

The down side is that cooling characteristics of this brake type are inferior, as the air flow is restricted into the disc internal channels. The air enters from the outboard side, through a small gap between the hat (hub) and disc ID, then must turn 90°, to flow radially through the channels towards disc OD. In addition, this disc experiences higher thermal stresses in the hat/disc transition region, when compared to the 'standard' disc design (where outboard face is attached to the hat section). The disc has 30 straight radial vanes and overall thickness of 45 mm, consisting of two 14 mm thick faces and 17 mm gap (channel width).

Table 1: Disc characteristics

Outer Diameter (OD)	Inner Friction Diameter (ID)	Rotor Thickness	Mass	Number of vanes
434 mm	234 mm	45 mm	38.5 kg	30

In this phase of the research, disc only investigations were conducted; as stated, investigations with the caliper and pads will be the subject of later studies. In all analyses within this paper, the brake disc was assumed to be heated uniformly to an elevated temperature, then kept stationary and cooled down in still air. Heat dissipation areas and associated modes are shown in Figure 2 (displaying scrap cross section of the disc) and detailed in Table 2. In all analyses shown in this Paper (Part 1), the disc ventilation system was closed by blocking the channel entry and exit areas with a temperature resistant tape (Figure 2). Furthermore, an insulating gasket was placed between the disc hat and wheel carrier flange, in order to minimise conductive heat transfer to a negligent level. The effect of this insulation is relatively minor and will be discussed in greater detail in Part 2 of the Paper.

In order to conduct the analyses effectively and with acceptable accuracy, all heat transfer modes have been considered and appropriately modelled.

3.1. Conduction

The heat is transferred by conduction between the disc and wheel carrier, through the contact area, the 'Flange attachment' marked in Figure 2. The fastening method is with 10 bolts M16, torqued to 330 Nm in the vehicle installation. Obviously, the heat can travel in either way but with the disc being most commonly at higher temperature, conductive transfer is mostly taking the direction from the disc into the wheel carrier. Due to irregularities of the surfaces in contact, there will be inevitable *thermal contact resistance* (R_{cond}) resisting the heat transfer and causing temperature difference between the interfaces. In practice, this phenomenon is best described using *thermal conductance* (h_{cond}) parameter, as used by various authors. In such a manner, heat (power) transferred by conduction (Q_{cond}) can be calculated using a simple formula:

$$Q_{cond} = h_{cond} A_{cond} \left(T_{d(int)} - T_{c(int)}\right) \quad (1)$$

Where h_{cond} is thermal conductance in [W/m^{2}K], A_{cond} is interface contact area in [m^2], $T_{d(int)}$ disc interface temperature in [K] and $T_{c(int)}$ carrier interface temperature in [K]. Thermal conductance is a function of interface surfaces conditions, materials and clamp force. The higher the conductance, contact area and/or interface temperature difference, the higher rate of heat transfer will be.

Tirović and Voller [9] experimentally established a relationship for calculating thermal conductance for this particular type of materials (grey cast iron disc and spheroidal cast iron wheel carrier), surface finishes and condition of contact surfaces. It important to bear in mind that the conductance is a function of interface pressure, hence its values will very across the interface. For bulk heat transfer, related to engineering calculations, average values are most appropriate, hence:

$$h_{conv(avg)} = 800 P_{avg} + 2300 \quad (2)$$

In the above formula $h_{cond(avg)}$ is obtained in [W/m^{2}K] for average interface pressure P_{avg} in [MPa]. The average interface pressure can be calculated by dividing the total clamp force (developed by 10 bolts) by the interface area. The clamp force can be calculated from the tightening torque of the bolts, which is straightforward. However, introducing conduction into simplified models will be quite difficult, and heat flow to/from the wheel carrier may change over long cooling times. Considering small conductive

contact area, this influence is unlikely to be very significant. It was therefore decided most appropriate, at this stage, to insert a thermal insulating gasket at the disc/carrier interface, as well as reduce bolt clap force (tightening torque) to a very low level, and assume that no heat transfer takes place across this joint. Experiments proved this assumption to be correct.

3.2. Convection

Convection is considered to be a dominant heat transfer mode in most braking duties, highly dependent on vehicle speed, hence requiring particular attention. In the case considered, i.e. disc rotational speed is zero, convective heat transfer will be the lowest possible. Furthermore, in driving conditions, there is relatively little influence of disc temperature on convective heat transfer coefficient. As fresh air is supplied to the surface, the drop of convective heat transfer coefficient with an increase in temperature is relatively minor. In stationary conditions, the situation is completely opposite, as only natural convection takes place. The only 'driving force' is disc-air temperature difference, the hotter the disc, the higher h_{conv} and also higher total heat dissipated. Furthermore, heated air raises and further influence local flows and heat transfer.

Convective cooling power (Q_{conv}) can be defined similarly to conductive cooling (1):

$$Q_{conv} = h_{conv} A_{conv} (T_d - T_\infty) \quad (3)$$

In the above formula h_{conv} is average convective heat transfer coefficient in [W/m^{2}K] for the entire disc wetted area A_{conv} in [m^2]. T_d is average disc temperature in [K] and T_∞ is ambient air temperature in [K]. No doubt that different disc areas will have different h_{conv} values, the temperatures T_d across large disc surfaces are also likely to vary. That makes convective cooling even more complex and necessary 'averaging' prone to assumptions, simplifications and errors. In Part 2 of the Paper, modelling using CFD will deal with more realistic and complex cases, including heat transfer from the disc ventilation system (channels and vanes), and give insight into local convective heat transfer coefficients and air temperatures in disc proximity. For this, initial stage aiming at analytical analysis, the ventilation system was blocked at the channel entry (disc inner diameter) and exit (disc outer diameter). This practically made the disc of a 'solid' design, still very important to understand and complex to analyse. It also

enabled the analytical solutions to be found and verified. Most of the paper will deal with convective heat dissipation, which will be dealt with in great detail.

Table 2: Heat dissipation modes and associated areas [m^2]

Conductive: Total A_{cond} = 0.02384	**Convective:** Total A_{conv} = 0.65767				
	Outer hat	Outboard friction	Inboard friction	Outer diameter	Ventilation system
	0.10379	0.10493	0.11958	0.01657	0.31280
	Radiative: Total A_{rad} = 0.34487				-

3.3. Radiation

Heat dissipation by radiation is typically associated with high temperatures and sometimes neglected but in this particular case of a stationary disc, it is of high importance, as the convective cooling is low. The basic formula of radiative heat dissipation Q_{rad} is well known:

$$Q_{rad} = \varepsilon\sigma A_{rad}\left({T_d}^4 - {T_\infty}^4\right) \quad (4a)$$

Where ε is the emissivity [-] of the disc surface, σ is Stefan-Boltzmann constant (approx. 5.67E-8 Wm^{-2}K^{-4}), A_{rad} in [m^2] is disc area emitting heat through radiation, T_d is average disc temperature in [K] and T_∞ is ambient air temperature in [K]. The only outstanding property needed is the emissivity (ε) of the disc surface. Radiation and emissivity in particular will be discussed in greater detail in the experimental work (Section 6) of this Paper, where an average emissivity value of ε = 0.92 was established as a value to be used for the modelling of this particular disc in the test conditions. More details about the method of establishing this value will be given in section 6.4.2, with experimental results. It should be also noted that disc area emitting heat through radiation A_{rad} is much smaller (see Figure 2 and Table 2) than convective area A_{conv} as there is no radiative heat loss to the environment form the ventilation system. When the brake is installed within the wheel cavity, boundary conditions become much more complex, as there will be radiative transfer to the caliper and wheel, as well as reflection from their surfaces. Some of these aspects have been studied by Voller [2]. In the considered case the disc was in free air, hence radiative heat transfer is much simpler to model.

The equation (4a) can be written in the same format as conductive (1) and convective (3) modes:

$$Q_{rad} = h_{rad} A_{rad} (T_d - T_\infty) \quad (4b)$$

Radiative heat transfer coefficient h_{rad} now becomes a function of emissivity and temperature:

$$h_{rad} = \varepsilon\sigma \frac{\left({T_d}^4 - {T_\infty}^4\right)}{(T_d - T_\infty)} \quad (4c)$$

3.4. Summary

Based on the previous considerations, analytical methods were used to predict convective heat transfer coefficients on disc friction surfaces and hat areas, which will be presented in the next section. Following that, disc brake temperatures were predicted by developing numerical models. Extensive experimental work was conducted on a specially developed Thermal Rig, where the disc was heated using induction heater and temperatures measured using contact and imbedded thermocouples. The experiments also enabled determination of the surface emissivity, for accurate prediction of the radiative heat dissipation. Finally, measured and calculated temperatures were compared for a cooling period which lasted 6 hours.

4. Analytical Investigation into Brake Disc Heat Dissipation

Analytical modelling of a CV brake disc geometry has not been presented in the literature thus far and therefore, no precedence on a method of generating accurate temperature predictions has been set. The approach taken here was to use a simplified brake disc geometry and generate a set of local h_{conv} values that could then be averaged across the whole friction surface. Equations from well-established literature were used to generate dimensionless parameters and then they were extrapolated over the simplified friction surface geometry partitions, as displayed in Figure 3. These values were then averaged across the whole surface area to generate an equation for the average h_{conv} over the specific temperature range relevant to CV parking applications. Finally, the same analytical method was applied to the hat region, by replacing vertical wall theory with the theory of heat dissipation from horizontal cylinders. The same approach can be applied to the cylindrical area at disc OD but this area is insulated and much smaller, hence can be neglected.

To simplify the process, it is assumed that all cooling transpires on the two heat transfer modes; convection and radiation, with a negligent amount of energy being transferred via conduction to the wheel carrier (as explained in the previous section). Subsequently, validation and accuracy testing will be conducted by comparing the analytical results with measured values.

Brake disc temperatures can reach in excess of 500°C after heavy brake applications, although it is unlikely that a CV would park after such an application. Less severe braking applications, on the other hand, frequently reach and exceed 400°C. Consequently, it was assumed that a parking application simulation would begin with a disc brake surface temperature at a maximum of 400°C, representing a realistic but harsh case.

4.1. Analytical Modelling of a Vertically Positioned Disc

Heat transfer research on natural convection has throughout history been completed on bodies with simple geometry. For example, McAdams [10] showed the generation of the thermal and hydrodynamic boundary layers of free air from a flat plate placed vertically and horizontally whilst Morgan [11] conducted similar work but with cylindrical geometry in free air.

The thickness of the rotor section is much smaller than the OD, meaning the majority of convective cooling transpires from the vertical friction surfaces. Therefore, it is reasonable to approximate the disc with two vertical plates in free air. Simply using standard equations proposed by both McAdams [10] and Churchill and Chu [12] would be difficult to justify as they calculated their equations based on rectangular plates in free air, where their characteristic lengths are considered constant.

Considering the friction surfaces of the disc brake are essentially ‘hollow circles’ (rings), using the straight vertical wall equations would also be inappropriate as the characteristic length changes continuously around the disc. Simplified disc geometry was necessary to enable an estimate of the heat dissipation patterns from the disc brake, with Figure 3 outlining the generation of the simplified geometry, followed by the subsequent flow analysis. The assumption that the friction surfaces could be separated into the four separate regions was made, as indicated in Figure 3. On either side of the disc, an area is made by an arc starting and finishing directly above and below the ID, located on the

horizontal centre line (in Figure 3). The height of the arc above the horizontal centre line, y_{arc}, was found using equation (5), based on Pythagoras's theorem.

$$\frac{dA_{arc}}{dx} = y_{arc} = (r_o{}^2 - x^2)^{1/2} \tag{5}$$

To find the area of the arc area, integration of equation (5) was completed. Limits of the integration were in the ***x*** direction, along the horizontal distance from the inner radius, r_i, to the outer radius, r_o. Obviously, the total arc area is the summation of the area above and below the horizontal centreline but equation (5) only calculates the height from the horizontal centreline. As the areas are symmetrical above and below, a doubling compensation factor has been added to the integration in equation (6). Integration was conducted by using the trapezium rule with a step size of 1 mm. Calculations of the individual areas gave the total arc area to be 0.0258 m^2.

$$A_{arc} = 2\int_{r_i}^{r_o} (r_o{}^2 - x^2)^{1/2} dx \tag{6}$$

With arc geometric properties now known, attention turned to the airflow patterns and heat dissipation across the arc, the first action was to access the heat transfer mode within the fluid. It is the Prandtl number (Pr), calculated by equation (7), that describes the relationship between the momentum dissipation of the fluid to the heat diffused to the flowing fluid. High Prandtl numbers are often found in oils where momentum diffusion is stronger than the thermal diffusion; consequently, thermal conduction is the predominant mode of heat transfer. On the contrary, Prandtl numbers are small in substances such as liquid metals, where convection is dominant [13]. The thicknesses of the velocity and thermal boundary layers are both dependent on the value of the Prandtl number, with small hydrodynamic boundary layers correlating to primarily convective cooling. The Prandtl number is independent of the surface interaction as it is a fluid only property.

$$Pr = \frac{C_p \mu}{k} = \frac{\mu \rho}{k/(\rho C_p)} = \frac{v}{\alpha} = \frac{Molecular\ diffusivity\ of\ momentum}{Thermal\ diffusivity} \tag{7}$$

Prandtl number (Pr) remains constant across the wall surface as it is independent from wall interaction and characteristic length. Increasing temperatures do however decreases the Pr value. It should be noted

that the fluid used throughout was air (temperature dependant air properties used were taken from [13]). The highest Pr value was generated at the lowest temperature of 20°C equalling 0.703. The lowest calculated Pr value was 0.688, a 2% drop at the maximum 400°C air temperature. These Prandtl numbers are below unity and are therefore considered a low value, specifying that convection is the main heat dissipation mode within the air passing over the solid brake disc.

4.1.1. Grashof Number

The Grashof number is a very important dimensionless parameter in buoyancy driven flow. Like the Reynolds number in forced convection flow, the Grashof number describes the ratio of fluid inertia forces to fluid viscous forces. When viscous forces are dominant, the flow is said to be in a laminar state, damping out potential eddy currents in the flow. As the inertial forces increase in significance, the flow goes through a transitional state before tripping into a fully developed turbulent flow. Inertia forces are now too strong to be dampened by the viscous forces. Small hydrodynamic boundary layers are present with turbulent flows, resulting in high convective heat transfer coefficients as the cooler fluid replenishment can occur more rapidly.

The Grashof number can be calculated by using equation (8) where g is the gravitational acceleration, ζ (often termed β) is the coefficient of thermal expansion [13], L represents the characteristic length of the body surface [14], T_w is the wall temperature of the solid and ν is the kinematic viscosity of the fluid.

$$Gr = \frac{g\zeta L^3(T_w - T_\infty)}{\nu^2} \tag{8}$$

Unlike the Prandtl number results, a significant change is seen across the horizontal centreline (Figure 3). At the r_i, where the local characteristic length was greatest, a value $5.08\text{x}10^8$ was calculated. This value reduces in the x direction across the arc, down to zero at the r_o because the characteristic length is zero. This is a very interesting result as it shows that airflow over parts of the arc could have transitioned into fully developed turbulent flow, or at least into the transitional phase, whilst laminar flow exists further towards the OD.

The calculated values of Gr assume the flow over the local vertical surface, with a specific characteristic length are independent of the flow horizontally adjacent to it. Eddy currents created by the perturbing flow towards the turbulent r_i cannot be expected to be only influencing the air perpendicular to the surface. Perturbations will create some lateral flow motion, affecting some of the laminar flow regions towards the laminar r_o. Without CFD analysis this effect cannot be investigated further due to the added difficulty in the mathematical formulations and the time constraints associated with the project. For now, the assumption that any turbulence flow will be confined perpendicular to the horizontal position on the disc brake surface will remain.

Interestingly, looking at a single point on the horizontal centre line, as the temperature drops, the magnitude of the Grashof increases until a maximum is reached at the temperature 255.6°C. Afterwards, the Grashof number falls until it reaches zero at ambient temperature when there is no thermal gradient present. This result is somewhat a surprise looking at equation (8) as the change in temperature is directly proportional to the Grashof number. The occurrence of the peak Gr value is attributable to the change in kinematic viscosity as Gr is inversely proportional to its square. As the temperature of a fluid increases, its density drops as thermal expansion occurs. Lower density fluid results in reduced friction within the flow, lowering the kinematic viscosity. Above the critical temperature of 255.6°C, the changing kinematic viscosity effects surpass the thermal gradient, thus and reducing the Gr value hereafter.

4.1.2. Rayleigh Number

When investigating heat transfer from a body subjected to buoyancy driven flow, the Rayleigh number is used in place of the Grashof number; calculated by multiplying the Grashof and Prandtl numbers (equation (9)). It represents the ratio of conductive heat transfer to convective heat transfer. Below the critical value, conduction is the dominant mode of heat transfer and reversing to convection thereafter. Depending on the situation and shape of the solid surface, the critical value of Ra varies. For example, McAdams [10] suggests the critical value for a flat horizontal plate is as low as 10^7 whilst Necati Özisik [13] proposes a value up to 10^9 for vertically placed cylinders in free air.

$$Ra = Pr.Gr \tag{9}$$

Considering the Rayleigh number is a function of the Grashof number, it is unsurprising that the results seen are of the same nature. A value of 3.49×10^8 at 400°C corresponds to turbulent flow according to McAdams [10]. The results show the air flow trips into a turbulent state just 8 mm from the OD. In contrast, the critical Ra value proposed by Necati Özisik [13] albeit for a different geometry, would suggest that the flow perpendicular to arc surface would be in a laminar regime throughout. Neither value derived was for the same surface geometry as the arc, making it impossible to tell by numerical calculation whether the flow has fully tripped into a complete turbulent regime. Ambiguity with the airflow state has made definite heat dissipation conclusions impossible to state, although the evidence would suggest the flow, at very least, will have reached the transitional period in between laminar and turbulent flows when the disc is at its hottest.

4.1.3. Nusselt Number

With the fluid properties now identified for flow over the arc surface, focus was placed on understanding thermal interaction from the wall to the fluid by calculating the Nusselt number, Nu. Finding the Nusselt number is not always as straightforward as inserting values into equation (10) usually because they are not all known. Small changes in geometry impact the intensity of the buoyant flow and subsequent parameter values. With the Nusselt number, it is often preferred to use approximation equations found by gathering experimental data and performing a correlation analysis on them. Necati Özisik [13] demonstrates the correlation method produces values closer to experimental results compared to theoretically derived equations. Various correlations have taken place for different solid surface configurations within buoyant fluid flowing over it. Churchill and Chu [12] provided a correlation equation for a vertical wall, valid for Rayleigh numbers between 10^{-1} and 10^{12} and when isothermal wall conditions are assumed.

$$Nu = \frac{h_{conv}L}{k} \tag{10}$$

Where the Prandtl number looks at the flowing fluid and the relationship of heat dissipation through it, the Nusselt number considers the ratio of convection to conduction energy transfer from the solid surface boundary to the flowing fluid and across its thickness, in a direction normal to the surface. Nusselt numbers at unity show an even distribution of conduction to convection heat dissipation from the surface, characteristic of laminar type flow. In convection dominant turbulent flow [13], values of Nu will rise above 100. It is important to note that the parameter L in equation (10) is the characteristic length of the body's surface.

Determination of the Nusselt number over the arc region will help describe the dominant mode of heat transfer. Two separate correlation equations have been presented by Churchill and Chu [12], equation (11) and McAdams [10], equation (12) to calculate the mean local Nusselt number; both were used and compared, as shown in Figure 4.

$$Nu_m{}^{1/2} = 0.825 + \frac{0.387 Ra_L{}^{1/6}}{[1 + (0.492/Pr)^{9/16}]^{8/27}} \tag{11}$$

A second equation proposed by McAdams [10] has been said to match experimental data more accurately by Necati Özisik [13]. The later equation takes the form:

$$Nu_m = cRa_L{}^n \tag{12}$$

where c is a constant and n is the exponent of Ra. Values of these two parameters are dependent on Ra; they are shown in Table 3.

Table 3: Parameters for the McAdams [10] relationship for $\boldsymbol{Nu_m}$

Flow Type	Range of $\boldsymbol{Ra}$	$\boldsymbol{c}$	$\boldsymbol{n}$
Laminar	10^4 to 10^9	0.59	$1/4$
Turbulent	10^9 to 10^{13}	0.10	$1/3$

Both methods of calculating the Nusselt number described produce mean Nusselt number values across the thermal boundary layer. A comparison of the two methods was completed, with the Churchill and Chu [12] method examined first. Nusselt numbers above 100 relate to a surface to fluid regime dominated by convection, whereas it can be said that conduction through the fluid and away from the surface is represented by values of one and below. It can be seen in Figure 4 that the Churchill and Chu [12] equation predicts a value of 70.7. Keeping with previous patterns, this value is somewhere in between the two critical values, demonstrating a transitional state. However, the value is still high, signifying that convection dissipates the majority of heat from the arc surface but with conduction still having an influential effect. The maximum calculated value was 72.4, located at the r_i where the characteristic length is greatest and when the temperature dropped to 251.8°C. This nonlinear characteristic fall shows that the Nusselt number is dependent on both the temperature and the location.

In comparison, the correlation equation derived by McAdams [10] produces a similar looking Nusselt number pattern across the arc surface (as shown in Figure 4 for Churchill and Chu, [12]). However, with Nu values calculated to be 80.6 at the maximum temperature, with a maximum of 82.5 at 251.8°C show the McAdams [10] equation produces values 14% higher. Even with the large increase in Nu, the heat transfer process from the arc surface still cannot be characterised as convection dominated. With both equations being based on experimental data, it was expected that a closer alignment between the generated results than what was actually achieved. According to Necati Özisik [13] the McAdams [10] equation is a closer approximation to actual value so will be used in all further calculations regarding vertical wall heat transfer calculations.

Having established that convection dissipates the majority of heat from the arc surface to the air, calculation of the convective HTC could transpire. Firstly, it must be stated that any calculation of h_{conv} will encompass the conduction effects from the surface to the air. In Figure 5 the locally calculated mean h_{conv} values, established from equation (10) are presented for different locations across the disc arc area. High variability is seen for h_{conv} values, ranging from zero to a maximum of 14.4 W/m^{2}K at the maximum temperature.

An increase in the thermal conductivity with temperature prevents the occurrence of a peak h_{conv} value as seen of the Nusselt number, at least within the region this project is concerned about. One pattern that is equivalent is the magnitude reduction as the characteristic length (height from centreline to the arc) decreases towards disc outer radius (r_o). This is an expected result because the characteristic length of the thermal boundary layer shortens, reducing the amount of heat transfer taking place.

4.2. Convective Heat Transfer over the Arc Area

With the data shown in Figure 5 it was possible to derive an equation relating to convective HTC with both temperature and location. It was unnecessary to develop such a complex equation as the aim was to produce a total surface relationship for a convective HTC. A single average h_{conv} value spanning the entire arc area was found through the use of equation (13).

$$h_{conv} = \frac{\sum_{i=r_i}^{r_o} h_{conv_i} A_{arc_i}}{A_{arc}} \tag{13}$$

Results of equation (13) were plotted against temperature in Figure 6, showing a highly nonlinear reduction in h_{conv} during cooling. A regression analysis was conducted on the results, using the post-processing program DIAdem, to obtain a relationship relating h_{conv} to temperature. A quadratic relationship, with a natural logarithm correction term, was found to deliver the optimum estimation as nearly 98% of the data was captured, see equation (14).

$$h_{conv} = a_1 + a_2 T_d + a_3 {T_d}^2 + a_4 ln(T_d) \tag{14}$$

The natural logarithm term was required to account for the decay as temperatures approached ambient. A regression equation describing over 99% of the data was achievable when ten higher order terms were included but it was decided the added accuracy was not justifiable considering the additional computational time that would be needed. Coefficients for equation (14) have been determined for the arc section and given in Table 4. The only caveat when using this equation is that is does not pass through zero at exactly at the point of ambient temperature. Therefore, for the purpose of future FE modelling, the user must manually input a zero h_{conv} value for the ambient temperature and then allow equation (14) to predict thereafter.

Table 4: Coefficients relating to equation (14) for the arc area

a_1	a_2	a_3	a_4
-10.65	-0.0251	3.42E-5	4.56

4.3. Convective Heat Transfer over the Rectangle Area

Of the four sections on the simplified disc brake friction surface geometry, convective heat transfer from the two rectangular sections remained undefined. By conducting a similar procedure for the arc areas, a disc brake friction surface h_{conv} equation could be generated. An advantage of being able to assume a rectangular shape is that the boundary layer on the surface normal would develop evenly across the surface, in the horizontal direction. Consequentially, the airflow and hence, the heat transfer properties across the section would be constant; this lack of dependency on local horizontal position greatly simplified the process.

Due to the construction of the simplified geometry, the base lengths of the rectangles are equal to twice the r_i dimension. Rectangle height, y_r, would be analytically calculated by equating the whole disc surface area to the four sections then rearranging for y_r. By doing so, the area of the simplified geometry was equal to the standard geometry, making them equivalent. Through the use of equation (15) the rectangle height was found to be 114.1 mm.

$$y_r = \frac{\left(\frac{\pi({r_o}^2 - {r_i}^2)}{4} - 2A_{rec}\right)}{2r_i} \tag{15}$$

Dimensionless numbers were calculated for the rectangle using y_r as the characteristic length of the wall. The temperature range being investigated will remain from 20° to 400°C with the same temperature dependent air properties. Figure 7 shows the change in Prandtl, Grashof, Rayleigh and Nusselt numbers with temperature. Prandtl values decrease with an increasing temperature; as air remains the fluid, the values match those given for the arc area. The Grashof, Rayleigh and Nusselt numbers all show the same fundamental characteristics as they started at zero and increased in a nonlinear fashion to a peak value before falling away thereafter; peak values were 1.68e7, 1.16e7 and

34.5 for the three varying dimensionless numbers respectively. Dimensionless values are much lower than those realised for the arc area as the maximum characteristic length y_r is much smaller. In contrast to the arc area, flow representative of laminar conditions is suggested for the air flowing over the rectangle area. Larger hydrodynamic boundary layers would be present here, resulting in lower HTCs than for the arc area.

Convective HTC result for the rectangular area demonstrate the same pattern seen for the arc area (shown in Figure 6), because the same equations and fluid properties were used, with a maximum value of 11.4 W/m^{2}K at 400°C, the h_{conv} value was lower than the arc area by 4.1%. The regression equation that predicts the h_{conv} values was in the same format as equation (14), with its coefficients given in Table 5.

Table 5: Coefficients relating to equation (14) for the rectangle area

a_1	a_2	a_3	a_4
-10.22	-0.0240	3.28E-5	4.37

4.4. Convection Heat Transfer Coefficient over the entire Disc Friction Area

Simplifying the brake disc geometry allowed two separate heat transfer investigation areas to be established for the disc friction surface. By taking a weighted average of the equivalent h_{conv} values, a generalised appreciation of the heat transfer variation with temperature was realised for the whole disc brake surface. The contribution of the arc surface area to the whole surface contact face area is 51%, making its weight function 0.51 with 0.49 being the resultant rectangle weighted function. A final disc surface regression equation is presented in Figure 8. Again, nearly 98% of the data is represented by the corrected quadratic equation; coefficient values available in Table 6.

Table 6: Coefficients relating to equation (14) for the disc friction area

a_1	a_2	a_3	a_4
-8.07	-0.0189	2.56E-5	3.45

Previous sections were devoted to achieving an equation that describes the convective heat transfer from the disc brake friction surfaces but the need for four terms in the h_{conv} equation pronounces the relative complexity of the behaviour. Many factors that influence the h_{conv} value had to be omitted or simplified in order to produce the relationship. For example, it was mentioned that the relative position on the surface was ignored. The presence of the hat section on the outboard side has been shown to affect the flow over the surface. Incorporating this effect would have dramatically increased the complexity of mathematical expressions. A final effect that was neglected was the air flowing over the top rectangle would be hotter than the bottom rectangle. Identical figures where used to calculate the top and bottom rectangle heat transfer values. Clearly, the symmetrical results generated will not be true to nature. Because all the simplifications made and interactions ignored, the h_{conv} equation made should be used for relatively crude calculations of heat transfer. However, this approach much improves the temperature prediction currently used for disc brakes under parked conditions. Furthermore, the convective heat transfer properties have been investigated from a generic disc shape geometry thus far, orientated vertically in free air. Consequently, this technique can now be applied to find the h_{conv} value for the hat section.

4.5. Convective Heat Transfer over the Hat Section

To complete the convection study on the CV disc brake, the same dimensionless number investigation, undertaken for the disc friction surface, was repeated on the hat section. Considerable research has also been devoted to buoyant air flow around cylindrical shapes. The considerable length and diameter of the cylinder shaped hat region of a CV brake disc allows a significant amount of convective heat dissipation to occur from this surface. As with flat walls placed vertically in free air, Churchill and Chu [12] correlated a trend in Nusselt numbers for cylinders from experimental results. Their correlation equation (16) is valid for isothermal surfaces only, for Rayleigh numbers falling within the range of 10^{-}

^{4} to 10^{12}, for flow over cylindrical bodies. The subscript D denotes the calculation of the Rayleigh number used the cylinder diameter for the characteristic length.

$$Nu^{1/2} = 0.60 + \frac{0.387{Ra_D}^{1/6}}{[1 + (0.559/Pr)^{9/16}]^{8/27}} = \left(\frac{h_{conv}D}{k}\right)^{1/2} \quad (16)$$

Morgan [11] also provided a correlation equation (equation (17)), it has the same form as the McAdams [10] equation for vertical walls, but with the coefficient values corresponding to the relevant Ra value range for flows over a cylindrical surface.

$$Nu = \frac{h_{conv}D}{k} = c{Ra_D}^n \quad (17)$$

The Morgan [11] equation, not only has the same form as the McAdams [10] equation but its coefficient values also have the same magnitude. Consequently, the dimensionless numbers are expected to have the same profile, varying only its scale because of the change in characteristic length (Table 7).

Table 7: Values for the Morgan [11] equation with $\boldsymbol{Ra_D}$ range

$\boldsymbol{Ra_D}$	$\boldsymbol{c}$	$\boldsymbol{n}$
$10^{-10} – 10^{-2}$	0.675	0.058
$10^{-2} – 10^{2}$	1.02	0.148
$10^{2} – 10^{4}$	0.850	0.188
$10^{4} – 10^{7}$	0.480	0.250
$10^{7} – 10^{12}$	0.125	0.333

Starting with the hat geometry, Figure 9 shows the cross section of the disc brake. The hat was assumed to be constructed of two separate cylinders located in free air allowing convective HTCs to be found by using the Morgan [11] equation (equation (17)). Cylinder 1 has a diameter of 283 mm and a length of 32 mm whilst Cylinder 2 has a diameter and length of 220 mm and 73 mm respectively.

Calculated values for the four dimensionless numbers for both cylinders are shown in Figure 10. The larger diameter of the second cylinder causes greater magnitudes for each of the dimensionless numbers

except for the Pr number due to being a function of fluid properties only, independent of surface interaction. The larger diameter is offset by the length of the second cylinder when calculating the convective HTC as Figure 11 shows virtually no difference for the two. Only a single h_{conv} equation was created by averaging the results. Continuity was kept with the equation format as it once again matches equation (14); coefficients are shown in Table 8.

Table 8: Coefficients relating to equation (14) for the hat area ('mean cylinder')

a_1	a_2	a_3	a_4
-7.37	-0.0100	1.22E-5	3.13

5. Disc Temperature Prediction: Derivation of Numerical Equation

So far convective heat transfer coefficients were derived for the disc rotor (friction surfaces) and hat (cylinder) areas. As explained before and shown in Figure 2, some simplifications were introduced, the major being blocking the ventilations system, by preventing the air inlet and outlet from disc ventilation channels. That made the study related to the solid disc. Furthermore, conductive heat dissipation was minimised by inserting thermal insulation gasket between the disc hub flange and wheel carrier. This enabled a much simplified approach, neglecting conductive heat transfer. As the first approach in thermal modelling, it was assumed that it is sufficient to consider disc rotor only, completely neglecting hat section. Although this might sound as a considerable shortcoming in modelling disc temperatures, experimental work proved the approach to be valid. It is interesting to note that at the beginning of the cooling period the hub (hat) is cooler and the heat is transferred into the rotor, with the internal conductive heat transfer changing direction during the cooling period. Actually, because the rotor is cooling quicker, it reaches lower temperature (about 80 minutes into the cooling) and the heat gets conducted from the hub into the rotor after this period, to be dissipated into the environment.

The simplification introduced, considering a rotor only model, made the initial temperature prediction easier as it could be assumed an equally heated rotor. In experiments, at the beginning of the cooling tests, average hub temperatures were about 100°C lower than average disc temperature.

Assuming the initial disc rotor temperature was 260°C, convective and radiative heat transfer coefficients, established in previous section, were introduced on rotor friction surfaces. No heat dissipation was modelled from the outer or inner diameters. As the cooling process of the stationary disc is very slow, it can be assumed that thermal gradients between rotor core and surface are very small, hence disc temperature can be described as a single, bulk value. Heat (energy) loss in a period of time is equal to the product of rotor mass, specific heat and temperature change for the time period:

$$\Delta E = m_d C_p \Delta T \tag{18}$$

Modelling of three individual cases was conducted, all of which were for the scenario of the disc rotor only. For each case, the initial differential equation started from the energy balance equation (18), with different assumptions being made to create three separate cooling 'cases'.

Case 1 used constant, average heat transfer coefficients for convection and radiation (for the temperature range modelled) throughout the cooling period. Case 2 increased the modelling complexity by allowing the radiation to vary with temperature. Case 3 allowed variability in both radiative and convective heat transfer coefficients with temperature, throughout the cooling period. Obviously, the last case is expected to give most accurate result but it is also most difficult to model.

To solve the equations presented, one of MatLab's inbuilt differential solvers was used. The decision to use the generic standard differential solver built into MatLab, rather than writing a specific numerical code, was made to allow greater effort to be directed towards achieving the aims of the overall project. MatLab has six inbuilt differential solvers to offer ode23, ode45, ode113, ode15s, ode23ts and ode23tb. The first three are explicit solvers whereas the later three are implicit. As implicit methods use both the current time-step result plus the future time-step to produce the result, they have a higher order of accuracy but inherently require greater computational resources. Providing that the function is not stiff, an explicit method would suffice, rejecting the three implicit solvers. A function is stiff if a solver is unable to solve the ODE unless the time-step is sufficiently small, drastically increasing the computational time.

The ode113 solver could also be rejected as it was designed to solve ODEs of multiple orders, leaving either the ode23 or ode45 1st ODE solver. Both remaining solvers are capable of estimating the error in the time-step during all iterations, making the solver as efficient as possible without losing accuracy in the results. This also means that the built-in solver used is likely to be more accurate than any programmed solver specifically made. The ode45 solver was chosen to run the numerical problems, as well as all future numerical analysis, as it is a more accurate solver due to having 4th or 5th order accuracy compared to only 2nd or 3rd order accuracy for the ode23 solver (depending on the problem).

Assumptions regularly used when dealing with dynamic braking applications will be used to demonstrate its inadequacy for parking applications. Both the radiation and convection dissipation modes will be held constant, corresponding to a lumped cooling model. This situation is well documented and generates the 1st ODE shown in equation (19), known as Case 1. Because both radiation and convection were assumed constant in this particular case, it was possible to lump both terms together into a total disc brake HTC ($h_{total} = h_{conv} + h_{rad}$).

$$\frac{\mathrm{d}T_d}{\mathrm{dt}} = -\frac{h_{total} A_d (T_d - T_\infty)}{m_d C_p} \tag{19}$$

Disc friction area A_d is identical for both modes of heat transfer as ventilation system was not included, just disc friction faces. A constant value was used for disc material (grey iron) specific heat, C_p = 420 J/kgK.

Radiation is highly nonlinear with temperature. It is expected that by allowing the radiation HTC to alter with the temperature drop, the cooling estimation will be more representative of actual disc brake cooling. To examine this hypothesis, equation (20) was derived by separating the convection and radiation terms from the lumped model seen in equation (19). Case 2 increased the cooling equation complexity by allowing radiation to vary with temperature whilst continuing to hold convection constant.

$$\frac{\mathrm{d}T_d}{\mathrm{dt}} = \frac{A_d}{m_d C_p}\left(h_{conv} T_\infty + \sigma \varepsilon {T_\infty}^4\right) - \frac{A_d}{m_d C_p}\left(h_{conv} T_d + \sigma \varepsilon {T_d}^4\right) \tag{20}$$

It has been demonstrated that a fully oxidised grey cast iron disc brake, as used in these experiments, has a constant emissivity value of 0.92 throughout the cooling phase, as detailed in section 6.4.2. Subsequently, 0.92 was used for the vale of emissivity in all calculations.

The final scenario, Case 3, was to allow both convection and radiation HTCs to vary over the cooling temperature range. Having found a relationship for convection in equation (14), it was possible to derive the final 1st ODE by substituting it into equation (20), to generate equation (21).

$$\frac{\mathrm{d}T_d}{\mathrm{dt}} = -\frac{A_d}{m_d C_p}\left[\left(a_1 + a_2 T_d + a_3 {T_d}^2 + a_4 ln(T_d)\right)(T_d - T_\infty) + \sigma\varepsilon\left({T_d}^4 - {T_\infty}^4\right)\right] \qquad (21)$$

Temperature predictions will be shown later, together with the experimental results, when the measured values will be compared with all 3 modelling cases considered, throughout the 6 hours cooling period.

6. Experimental Investigations

6.1. Thermal Rig, Equipment, Instrumentation and Operation

6.1. 1. Thermal Rig and Equipment

Experiments were conducted on a specially developed and carefully commissioned Thermal Rig. It consists of an inline configuration of a 7.5 kW electric motor, shaft with bearing housing, torque and speed sensor. It holds a CV trailer axle, modified to enable experimentation on a complete brake assembly (disc, pads and caliper), as well as the wheel carrier and wheel. The Thermal Rig is located in Cranfield University, in the laboratories of the Department of Automotive Engineering.

Numerous sensors were deployed onto the Thermal Rig for testing to capture various aspects. For the experiments presented here, rubbing thermocouples were placed on the disc friction surface and a further three probe thermocouples were imbedded in the disc hat section (Hat 1, Hat 2 and Hat 3), as shown in Figure 12. A thermal insulating gasket, inserted between the disc and wheel carrier, is also shown, used to minimise heat conduction from the disc into the wheel carrier. The wheel (not shown) can cover the entire assembly and is mounted on the ten studs located on the wheel carrier, and secured with suitable nuts.

Initially, 20 rubbing/contact thermocouples were placed on each side of the disc friction surface (Figure 13a), covering over 180° of the disc friction area, with the other half being covered by the induction heater. Numerous experiments were conducted and it was concluded that there is no need to use so many thermocouples as the disc has large thermal capacity and, with cooling rates in still air being very low, disc material thermal conductivity and cross section being high, there is practically no thermal gradients that can be reliably measured over the disc surface. It is perfectly acceptable to use only 3 top thermocouples (per side), as shown in Figure 12 (for the outboard side). It is also worth pointing out that the thermocouples, mounting brackets and induction heating coil has no measurable influence on disc cooling.

Rubbing thermocouples (Figure 12 and 13) and probe/imbedded thermocouples used (Hat 1, 2 and 3 in Figure 12) were K type, which are suitable for measuring a large range of temperatures, from approximately -200°C to 1300°C.

6.1.2. Measurement and Data Logging Equipment

To collect data from the experiments various measuring instruments were used on or around the test rig. To collect and control these instruments, a variety of National Instruments (NI) products were used, with the individual modules and their characteristics explained below.

CompactRIO

The CompactRIO is an embedded controller which allows real-time data acquisition and instrumentation control. By combining the CompactRIO with the NI cRIO-9112 chassis, eight individual modules could be used simultaneously for data logging or control purposes. Utilisation of on board FPGA processors enables the CompactRIO to sample at multiple frequencies.

Thermocouple Modules

Three different module types were used to capture the temperature readings from the thermocouples in the CompactRIO; they were the NI 9211, NI 9213 and the NI 9214. The generated signal produced by thermocouples actually follows a 9th order polynomial pattern [15]. All three thermocouple modules

are controller by the LabVIEW program. The linearization of the thermocouple signal is conducted within LabVIEW.

The NI 9211 is the simplest of the three thermocouple modules. It is a straightforward analogue voltage reader, sensitive enough to detect the small voltages changes generated by the dissimilar materials in the thermocouple wire. The voltage range for the NI 92111 is ±80 mV. Up to four thermocouples can be logged simultaneously with this module, at a maximum sampling rate of 14 Hz, with a resolution of 24 bits. According to the specified data sheet, the NI 9211 has a maximum uncertainty of 1.3°C [16].

The NI 9213 module is very similar to the NI 9211 but the number of available channels to record is increased from 4 to 16. The ability to sample at a higher frequency was also added, 75 Hz if all 16 channels are being used or 100Hz if 12 or less are used [16]. An increase in the uncertainty was also quoted for the NI 9213 to be 1.8°C.

Finally, the improved NI 9214 thermocouple module was also used, enabling 16 channels of recording with a high degree of accuracy. According to [15], a K type thermocouple will output 20.6 mV when heated to 500°C. A stated accuracy range [16] of ±36 μV is representative of an uncertainty 0.85°C, at 500°C.

LabVIEW Program

LabVIEW program was developed for data acquisition and Rig control. Thermal Rig operation and disc testing can be essentially considered in three phases; Heating, Thermal Stability and Cooling. During Heating Phase the disc rotates slowly, typically at constant rotational speed of about 50 rpm, to ensure uniform heating, avoiding hot spots but also excessive convective heat loss. Rotation is provided by the three phase electric motor, with heat provided via an induction heating system (see Figure 12). The induction heating system is specifically designed for non-contact heating, resulting in repeatable experiments whilst being very efficient in heating the brake disc to over 400°C in less than 10 minutes.

During the Thermal Stability phase, the induction heater is switched off but the disc continues to rotate at low speed, in order to equalise the temperature distribution across the disc. A heating sequence was

developed which consisted of 5 heating cycles that took the brake disc friction surface to 400°C, followed by 5 minutes of Thermal Stability periods to equalise brake disc temperatures. On the conclusion of the sixth heating cycle, rotation was ceased and the Cooling phase begun. Temperature, speed and other data was logged throughout the three phases but only in this final phase was the actual measurement being conducted.

6.2. Uncertainty analysis in temperature measurements

Numerous experiments were conducted throughout this investigation. However, it is inevitable that the measured values for variables were not the "true" value as an amount of error is always associated with experimentation. As described by Moffat [17], *"the error in a measurement is defined as the difference between the observed value and the true value of the intended measured."* This definition can be defined mathematically by equation (22).

$$X = X(measured) \pm \delta X \tag{22}$$

The true value is represented by the term X, the measured reading is $X(measured)$ with δX being the difference between the two. Calculation of equation (22) delivers a precise value of a specific reading, yet the value of δX is often never known, making it impossible to find the true value. A large part of the problem is the correct identification of the type of error.

The meaning of the term "true" value is not as straightforward as one may think, as described previously by Moffat [18]. Examining the result an instrument produces will highlight the issue. For instance, taking the use of a thermocouple as an example, the reading at the junction of the thermocouple and the solid surface can be said to be the estimate of the true value (T_1); this is an intrinsic error. However, there is usually an amount of gas flowing over the surface, cooling the thermocouple junction slightly. Even though the cooling may be small, the second estimate of true temperature (T_2) should account for this. Interaction with of the measuring equipment and non-experiment specific conditions (i.e. with the surrounding air) is known as sensor interaction. Further refinement is made if the amount fluid of air passing over the surface is calculated as if the thermocouple was not there (T_3). At some point a judgement is needed to say what the true value estimation is being taken as. In the case of this

investigation, intrinsic errors only for any of the measuring systems will be used as the true value estimation; as seen for (T_1).

Uncertainties during experimentation are generated generally in two forms, random uncertainties and systematic uncertainties. Systematic uncertainties are functions of the experimental process, producing an element of bias to the results, whereas random errors occur, as the name suggests, in a random manner. Statistical analysis can be conducted on random errors, allowing an element of correction or justification to their reading. Conversely, systematic errors cannot be detected by statistical means and therefore present the danger of generating conclusions based on inadequate data. Efforts must be taken to ensure all experimental procedures minimise any systematic uncertainties. Systematic uncertainties that can be measured are those of created from the experimental instrumentation.

With temperature measurements being the predominant experimental reading taken in during this investigation, it is important to understand the uncertainty associated with thermocouple system. As stated previously, the uncertainty for individual thermocouples is known. However, the thermocouple system comprises of more than just the physical thermocouple, with uncertainties propagating though. The total uncertainty is calculated by addition of the uncertainties at each stage of the process, generating an overall system uncertainty. In the case of the thermocouple, there is a junction box coupling connecting the thermocouple and the cable, δX_{junc}, a connection between the cable and the thermocouple module in the CompactRIO, δX_{conn}, the thermocouple module itself located in the Compact RIO, δX_{NImod}, as well as the thermocouple, δX_{thermo}, to consider.

$$X = \bar{X} \pm \left(\delta X_{thermo} + \delta X_{junc} + \delta X_{conn} + \delta X_{NImod}\right) \quad (23)$$

Two of the uncertainty terms displayed in equation (23) are known from earlier work; δX_{thermo} and δX_{NImod}. Through experimentation, Nakos [19] found that provided there is no temperature gradient through the thermocouple/cable junction then the uncertainty in the recorded measurement is so small it can be neglected, due to the connector pins being of lesser quality material than the thermocouple cable. By assuming that this is the case for the experiments conducted in this investigation, the δX_{junc} term in equation (23) can be disregarded. This assumption is valid to make as there is sufficient length

of thermocouple wire, enabling the junction boxes to be kept out of the range necessary to produce sufficient heat transfer that would cause a gradient across it. Nakos [19] also investigated the uncertainty for the connection between the cable and a National Instruments terminal block. A conservative uncertainty value of ±0.8°C was suggested. Although the equipment used was different to that used here, the same value will be used as the connection from the various modules from National Instruments are very similar, which will cause the uncertainty to be fairly similar. In addition, as the value was described as conservative anyway, it can account for a potential slight increase with different modules.

With three thermocouple modules used in the CompactRIO, there were three different values of thermocouple uncertainty that needed to be calculated. Stating with the NI 9211, values of 2.2°C, 0.8°C and 1.7°C for δX_{thermo}, δX_{conn} and δX_{NImod} respectively, were put into equation (23).

$$X = \bar{X} \pm 4.7°C \tag{24}$$

A total uncertainty of ±4.7°C was found for the thermocouple system, using the NI 9211. Unfortunately, this value seemed to be too conservative, which could potentially lead to valid results being rejected on the basis on uncertainty. Thankfully, there was a set of results to compare to that will clarify whether this uncertainty estimate is indeed too conservative. Figure 14 displays the overall thermocouple system error when using K type thermocouples with the NI 9211 module [16]. Instrumentation used in the production of this graph were calibrated to a high level. It was shown that the uncertainty range for the temperatures in this investigation was considering between 2.2°C and 2.5°C, approximately half the value calculated. Consequently, it is confirmed that the calculated value in equation (24) was too conservative. Therefore, the values shown in Figure 14 were used.

It is a similar case for the other two thermocouple modules. An uncertainty value of ±4.8°C was calculated for the NI 9213 module, with the NI 9214 generating an uncertainty of ±3.8°C. A big difference is found with the final thermocouple as the uncertainty range displayed in Figure 15 is between only 0.35°C and 0.45°C. A discrepancy is presented here as this value is much lower than what Nakos [19] found for the thermocouple uncertainty by itself, let alone for the full system.

Taylor [20] describes the benefit of using multiple readings where possible to minimise the overall uncertainty in the data. In nearly all cases, where multiple data points have been collected, taking the mean of the data produces the best estimate of the true value. Equation (22) has to be altered slightly to accommodate the change to multiple measurements rather than a single reading. Therefore, $X(measured)$ can be replaced with $\bar{X}$, which represents the best estimate of the true value that can be made from the data.

Likewise, a change in the uncertainty term is also needed. The standard deviation, σ, is calculated from the differences each measurement in the set is from the mean, thus characterising the average uncertainties. Small values of σ show the experiments are precise whilst large values are obviously not precise. The uncertainty term in equation (22) is now replaced with the σ, giving a 70% statistical confidence that the true value lies within this range. Equation (22) therefore becomes (25).

$$X = \bar{X} \pm \sigma_X \tag{25}$$

Increasing the uncertainty term to $\pm 2\sigma_X$ improves the confidence that the true value has been captured, from the measurement set, to 95%. Therefore, the final uncertainty equation for a multiple data set is outlined in equation (26), provided the value of systematic uncertainties is much lower than this.

$$X = \bar{X} \pm 2\sigma_X \tag{26}$$

The discrepancy between the work produced Nakos [19] and the NI 9214 datasheet [16] previously discussed will be countered by using the $\pm 2\sigma_X$ method of uncertainty calculation. High confidence in the results is obtained without over or under predicting the experimental uncertainty.

It should be pointed out here that accurate *absolute* temperature value is of relatively little importance, as the equations extracted and comparisons made relate to the *relative* temperature change. With long cooling times and slow temperature changes it is important to have a stable system, rather than a precise one. Systematic errors of several degrees will have no practical influence on the actual equations

derived and HTC values obtained, as these were calculated for temperature ranges (more details are given in Part 2 of the Paper).

6.3. Measurement Results

To match the assumptions made during the analytical and numerical derivations, a gasket was placed between the disc brake and wheel carrier, and the vanes were blocked at the inlet and outlet, as showing in Figure 2. The former action minimised conductive heat transfer, the latter enforced convective cooling from the external surfaces only. By preventing in-channel cooling essentially made the disc non-ventilated (solid). The rubbing thermocouples measured the temperatures on the friction surface (see Figures 12 and 13); the average of these was used as the average bulk rotor temperature. Likewise, the three probe thermocouples inserted into the hat section (Figure 12), in the axial direction, recorded the temperature gradient in this region of the brake disc. A bulk hat temperature was generated by taking the corresponding averages of these values.

Figure 16 displays bulk rotor and hat temperatures, measured using the equipment and methodology described (see Figures 12 and 13). By averaging the friction surface temperature and the hat temperature, a value for the initial bulk (entire) disc temperature was taken as 257.8°C, which fell to 29.5°C over the six hour cooling period; it should be noted that the average ambient temperature during these experiments was 24.1°C. An interesting observation can be made; despite a higher initial temperature of the disc rotor, after approximately 80 minutes, the rotor becomes cooler that the hub. This is due to higher rate of heat dissipation from the rotor than hub surfaces. Consequently, after this time internal conductive heat transfer within the disc changes direction. Initially the heat was being conducted from warmer rotor into a cooler hub, thereafter from the hub into the rotor.

6.4. Disc testing – Heat Dissipation Modes

The work in this paper concentrates on convection losses, and has been conducted both theoretically and experimentally; however, the other two modes of heat transfer, conduction and radiation must not be neglected and could have been only studied experimentally. After suitably estimating heat dissipation by these two modes, convective heat dissipation has been addressed. Numerous tests were conducted

and tests conditions varied to ensure the assessments are accurate and tests repeatable. To achieve high level of confidence, the disc heating and cooling was conducted with and without the insulating gasket, disc vanes were open but also blocked (taped) to prevent air flow through the channels, disc surface condition was varied from newly machined (shiny) disc to fully corroded, as a result of repeated heating and cooling in ambient (laboratory) conditions.

6.4.1. Conduction

Figures 2 and 12 show the thermal insulating gasket used to reduce heat conduction into the wheel carrier. The methodology of determining conductive losses have been studied in detail by Tirovic and Voller [9]. It should be pointed out that conductive heat transfer mode is not speed dependent and Voller et al. [5] demonstrated that conductive losses can be considerable for some disc designs and specific conditions of contact surfaces. However, to provide simplified modelling conditions, a thermal gasket was installed between the disc and wheel carrier and clamp forces were kept low. Under these conditions, it was concluded that conductive losses are negligible. This was the result of experimental investigations and FE modelling (were disc and wheel carrier models were created and corresponding HTC applied). It should be also taken into consideration that conductive contact area is very small. Further experimental results on disc conductive heat transfer will be given in Part 2 of the Paper, with further details presented by Stevens [21].

6.4.2. Radiation

Heat dissipation by the mode of radiation, by definition, is highly variable with temperature, as there is a fourth order relationship between the surface and ambient (absolute) temperatures. It is also speed independent. The only outstanding property needed is the emissivity (ε) of the disc surface. Voller et al. [5] have demonstrated the large range of emissivity values used in the literature, for multiple disc brake materials and conditions. Following own measurements, it was predicted, for a similar disc design, for disc temperature of 600°C that radiative heat dissipation equals to 5 kW, and is higher than convective mode for vehicle speeds up to 35 km/h. That means that for stationary vehicle, even for lower temperatures, radiative heat losses can be quite considerable, higher than convective cooling.

Consequently, this mode of heat transfer cannot be neglected, and further research is required in appropriately defining its contribution to disc cooling. Some initial results have been already reported by Stevens et al. [22].

Emissivity (ε) is a property that describes a body's ability to accept and radiate electromagnetic waves. An indirect measurement technique was therefore used to generate reliable values for this property. By utilising a FLIR A320 infrared camera in conjunction with thermocouple temperature measurements, the emissivity of the brake disc was determined.

The FLIR processing software ThermaCAM Researcher was utilised for emissivity calculations, which required the physical temperature readings to be imported into the software. By using an iterative method of selecting a value of emissivity, the IR camera temperatures from the location SP01 (shown in Figure 17) could be matched to the recorded physical temperatures from the +000 DOO thermocouple. A limitation of the FLIR A320 camera and its corresponding processing software was that the temperature ranges it was capable of recording were from 0°C to 350°C and 200°C to 1000°C. Seeing as the temperature range under investigation throughout this project is from 20° to 400°C, the cooling test had to be conducted twice to capture data over the entire cooling phase (an obviously repeated to ensure consistent values are obtained).

Figure 18 displays the results of the emissivity testing, with the red markers for the higher range and green markers for the lower. Emissivity changes with temperature as the potential to accept electromagnetic waves diminishes as a body gets hotter. Figure 18 does indeed show this pattern, but the decrease with temperature is so minor, the difference it will make for calculation is negligible. Therefore, it can be assumed that the emissivity of the grey cast iron disc brake, is constant throughout the stationary parking application. It should be noted that this test was only conducted on the one brake disc, which was in the fully oxidised state. The oxidisation was a consequence of repeated heating to high temperature using non-contact induction heater. In actual driving conditions, with pads rubbing over the disc, it is likely for the emissivity values to vary. Consequently, this assumption can only be made for disc brakes that match this condition. Emissivity values shown in Figure 18 were taken at 10°C intervals, starting from 50°C up to 400°C. By averaging all the values, a mean emissivity value

of 0.92 was found. The minimum and maximum emissivity values calculated were 0.912 and 0.946 respectively. The values may seem high but they correlate well with the literature data which typically state values of around 0.9 for heavily corroded, machined cast iron surface. For instance, the source [23] quotes the emissivity $\varepsilon = 0.95$ for strongly oxidised cast iron surfaces in the temperature range between 40°C and 250°C. It should be noted here that after repeated heating in free air using (non-contact) induction heater, the disc surfaces get covered in a fine and smooth, 'velvet like' oxidised layer. These 'oxidised' surfaces should be distinguished from 'rusted' surfaces which tend to have lower emissivity values.

ThermaCAM Researcher required a set of parameters to feed into the software to help it decipher the image taken by the FLIR A320 IR camera. For instance, the intensity of the light received by the camera is a function of how far the camera was away from the targeted surface. For the photo taken in Figure 17 the camera was position 0.9 m away from the outboard disc brake fiction surface. Other important factors the software needed were the ambient temperature, relative humidity and the reflected temperature. Ambient temperature in the laboratory was approximately 20°C on the day of testing, so this value was used. It was also used for the reflected temperature value. To test the importance of the humidity reading, the change in calculated emissivity readings was assessed when values of 50% and 90% were used. A difference of less than 0.5% in emissivity values were calculated for the 400°C surface temperature, indicating that calculations are insensitive to the humidity. A predicted value of 70% relative humidity was used in the end calculations.

7. Model validation

As pointed out earlier on, heat transfer coefficient values will be further discussed in Part 2 of the paper, where analytical, experimental and CFD results will be presented and compared. In this section, analytically predicted temperature will be compared with measured values, over the entire 6 hours cooling period.

Figure 19 shows a comparison of the three numerical analysis results (as explained in Section 5) compared to experimental data, with 10% error bars inserted to represent the targeted accuracy level.

This was considered sufficient level for this stage of the Project. For the first hour very little difference between the predicted temperature profiles was seen for Cases 2 and 3, whereas the Case 1 clearly over predicts the temperature by more than the permitted limit. The main difference between Cases 2 and 3 occurs after the hour mark, when the two profiles separate. For Case 2, using a constant h_{conv} caused the temperature profile gradient to change less quickly than Case 3 once the disc brake had fallen below 125°C. Both methods remain within the 10% error limit but the ability to vary the convection made Case 3 qualitatively matches the cooling profile better than Case 2. It can be concluded that having a variable convection coefficient is important for maintaining the surface temperature cooling profile integrity during the transition from higher to lower temperatures.

The increase in h_{conv} at the low temperature end can be attributed to the variability in the radiation as little energy can be radiated as the temperatures approach the ambient. Keeping radiation constant in the previous case gave an overestimation of emitted radiation energy, consequently producing an undervaluation of the convection. It can therefore be concluded that the change in radiative heat transfer with temperature must be considered highly significant as its presence in the cooling 1st ODE improved the quality of the numerically generated results.

Although an improvement is evident, it cannot be said that the numerically generated cooling profiles match the experimental profile quite well for the final, Case 3 where both radiation and convection varied with temperature. Still, Figure 19 indicates lower predicted cooling for approximately the first three hours of the test, with higher rate of cooling thereafter. The maximum difference between the predicted and measured temperatures is approximately one hour into the cooling period.

8. Conclusions

As stated earlier on, the research presented has two automotive applications: the EPB development for commercial vehicles (where more complex models and instrumentation can be used), and for establishing a simplified, yet robust and accurate on-board ‘thermal model’, for temperature predictions and EPB control (clamp force, re-clamping etc.) on actual, production vehicles. In this, first phase, the focus was on brake disc, with the pads and caliper to be added later.

The geometry used in this study was of a simple disc, which in addition to automotive applications is also representative of any generic solid disc in free air; therefore this method is suitable for alternative industrial and other practical uses.

In this paper, Part 1, analytical modelling of a stationary disc cooling in still air was conducted from first principles. Numerical modelling using MatLab was required for establishing convective heat transfer from main disc areas, as well as for predicting disc temperatures during cooling.

Specialised experimental installation, Thermal Rig, enabled tests to be conducted on the actual disc, under controlled conditions. A powerful, 15 kW induction heater was used to uniformly heat the disc at low rotational speeds, with cooling tests conducted for stationary disc in still air. High repeatability of tests was achieved, with cooling curves being practically identical in repeated experiments. Conducted uncertainty analyses ensured further confidence in the results obtained. Investigations into radiative cooling demonstrated constant disc surface emissivity of $\varepsilon = 0.92$.

Predicted disc temperatures matched reasonably well to measured values throughout the 6 hour long cooling period, being within the 10% acceptable error. As expected, the best match was achieved when convective and radiative heat losses were modelled as a function of temperature. Numerical solutions calculated in MatLab, demonstrated that having fully variable boundary condition produces not only accurate results, but generates a cooling profile of the right qualitative nature as well. Heat transfer coefficients and temperatures investigated in this section were averaged over the main disc surfaces, which certainly has practical application for on-board vehicle prediction tools.

To enhance the understanding of heat dissipation from a CV brake disc, CFD modelling is required to explore flow patterns and h_{conv} variation over the whole disc brake surface area, throughout the cooling period. This is the subject of Part 2 of this research. Together with further experimental work, the aim is to establish and validate effective modelling techniques for predicting heat transfer coefficients for all disc areas.

Acknowledgement

The authors would like to acknowledge and thank Meritor HVBS (UK) and Engineering and Physical Sciences Research Council (EPSRC) for co-sponsoring the research project though EngD scheme. Special thanks to Jonathan Jackson, Dr Ralf Leiter, Paul Roberts, Martin Taylor and Peter Gibbens at the Meritor Cwmbran facility. Thanks also go to Dr Stewart Chidlow, a Cranfield University colleague, for his help with MatLab modelling.

References

1. Slosarczyk K, Linden J, Burnham K, et al. Implementation of an electronic park brake feature with limited data availability. In: *International Conference on Systems Engineering*, Las Vegas (USA), 2008.
2. Peng Y and Li W. Research on fuzzy control strategies for automotive EPB system with AMESim/Simulink co-simulation. In: *Control and Decision Conference*, Shanghai (China), 2009.
3. Lee C, Chung H, Lee Y et al. Fault detection method for electric parking brake (EPB) systems with sensorless estimation using current ripples. *International Journal of Automotive Technology,* vol. 11, 2010, 387-394.
4. Galindo-Lopez CH and Tirović M. Understanding and improving the convective cooling of brake discs with radial vanes. *Proc IMechE Part D: Journal of Automobile Engineering,* vol. 22, no. D7, 2008, 1211-1229.
5. Voller GP, Tirović M, Morris R et al. Analysis of automotive disc brake cooling characteristics. *Proc IMechE Part D: Journal of Automobile Engineering,* vol. 217, no. D7, 2003, 657-666.
6. McPhee AD and Johnson DA. Experimental heat transfer and flow analysis of a vented brake rotor. *International Journal of Thermal Sciences,* vol. 47, no. 4, 2008, 458-467.
7. Liang L, Jian S and Xuele Q. Study on Vehicle Braking Transient Thermal Field Based on Fast Finite Method Simulation. SAE paper 2005-01-3945, 2005.
8. Bagnoli F, Dolce F and Bernabei M. Thermal fatigue cracks of fire fighting vehicles gray iron brake discs. *Engineering Failure Analysis,* vol. 16, no. 1, 2009, 152-163.

9. Tirovic M and Voller GP. Interface pressure distributions and thermal contact resistance of a bolted joint. *Proceedings A of the Royal Society-Mathematical Physical and Engineering Sciences,* vol. 461, no. 2060, 2005, 2339-2354.
10. McAdams WH. *Heat Transfer*, McGraw-Hill, 1954.
11. Morgan VT. The Overall Convective Heat Transfer from Smooth Circular Cylinders. *Advances In Heat Transfer,* 1975, 199-264.
12. Churchill SW and Chu HHS. Correlating Equations for Laminar and Turbulent Free Convection from a Horizontal Cylinder. *International Journal of Heat Mass Transfer,* 18(9), 1975,1049-1053.
13. Necati Özisik M. *Heat Transfer A Basic Approach.* McGraw-Hill, 1989.
14. Richardson PD. Studies of Flow and Heat Transfer Associated With a Rotating Disc. *Mechanical Engineering Science,* vol. 5, no. 4, 1963, 336-342.
15. NIST ITS, *Thermocouple Database (1999)*: http://srdata.nist.gov/its90/main/its90_main_page.html, (accessed 10/08/2011).
16. National Instruments (Datasheets: NI 9211, NI 9213, NI 9214): www.ni.com. (accessed 10/08/2011).
17. Moffat RJ. Describing the Uncertainties in Experimental Results. *Experimental Thermal and Fluid Science,* vol. 1, no. 1, 1988, 3-17.
18. Moffat RJ. Using Uncertainty Analysis in the Planning of an Experiment. *Journal of Fluids Engineering-Transactions of the Asme,* vol. 107, no. 2, 1985, 173-178.
19. Nakos JT. Uncertainty Analysis of Thermocouple Measurements Used in Normal and Abnormal Thermal Environment Experiments at Sandia's Radiant Heat Facility and Lurance Canyon Burn Site. *SAND2004-1023*, 2004.
20. Taylor JR. *An Introduction to Error Analysis The Study of Uncertainties in Physical Measurements.* University Science Books, 1982.
21. Stevens K. *An Investigation into Heat Dissipation from a Stationary Commercial Vehicle Disc Brake in Parked Conditions.* EngD Thesis, Cranfield University, UK, 2013.
22. Stevens K, Leiter R, Taylor M et al. Thermal Aspects in Electronic Parking Braking of Commercial Vehicles. In: *European Conference on Braking*, Lille, France, 2010.

23. -Mikron:http://www-eng.lbl.gov/~dw/projects/DW4229_LHC_detector_analysis/calculations/emissivity2.pdf, accessed (10/03/2017)

List of Figures:

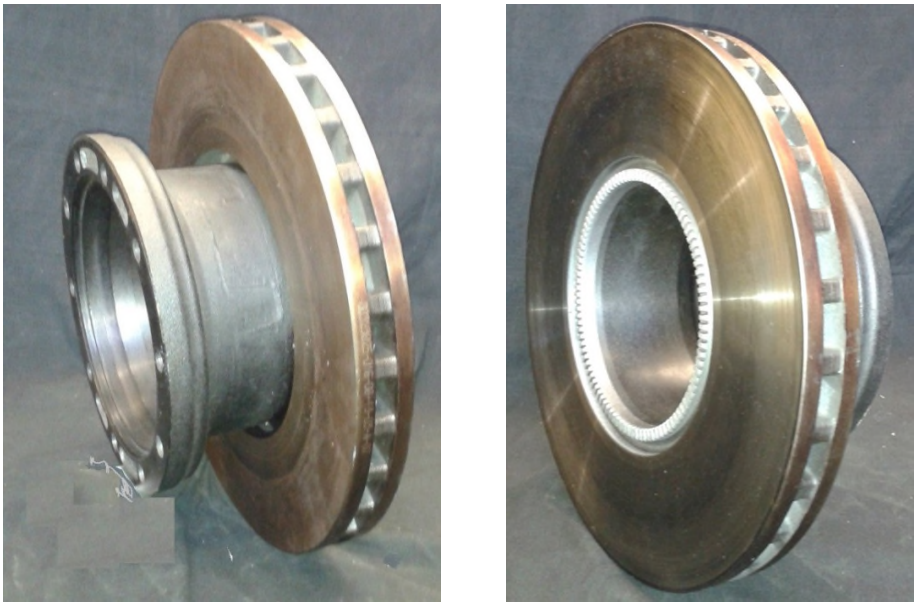

a) b)

Figure 1: Brake disc analysed: a) Outboard view; b) Inboard view

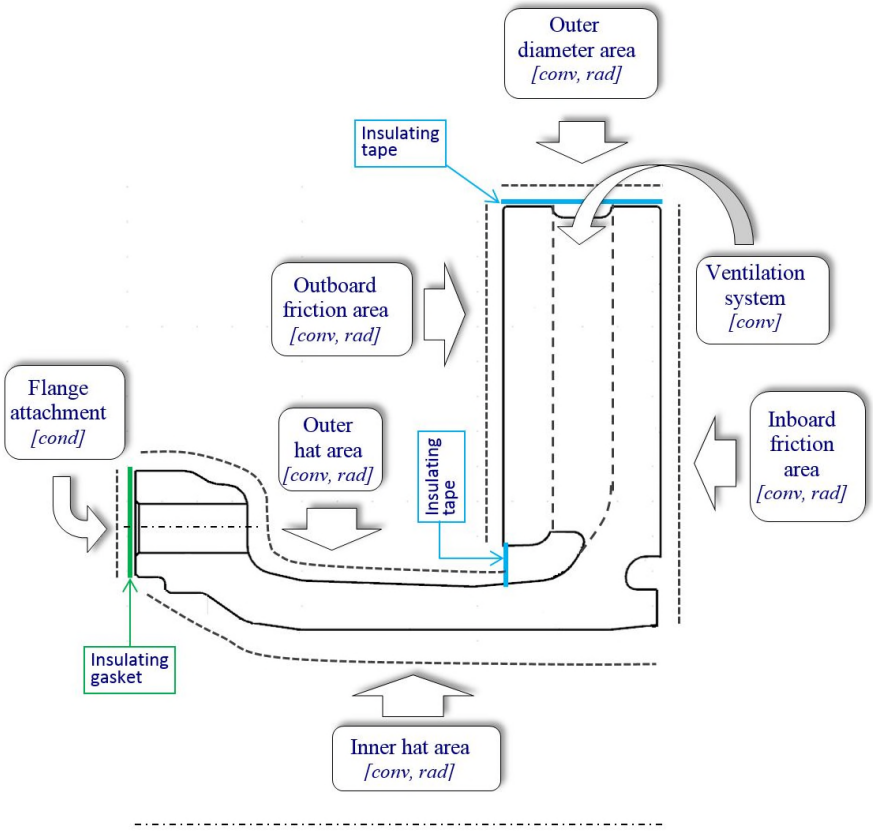

Figure 2: Disc areas and associated heat dissipation modes

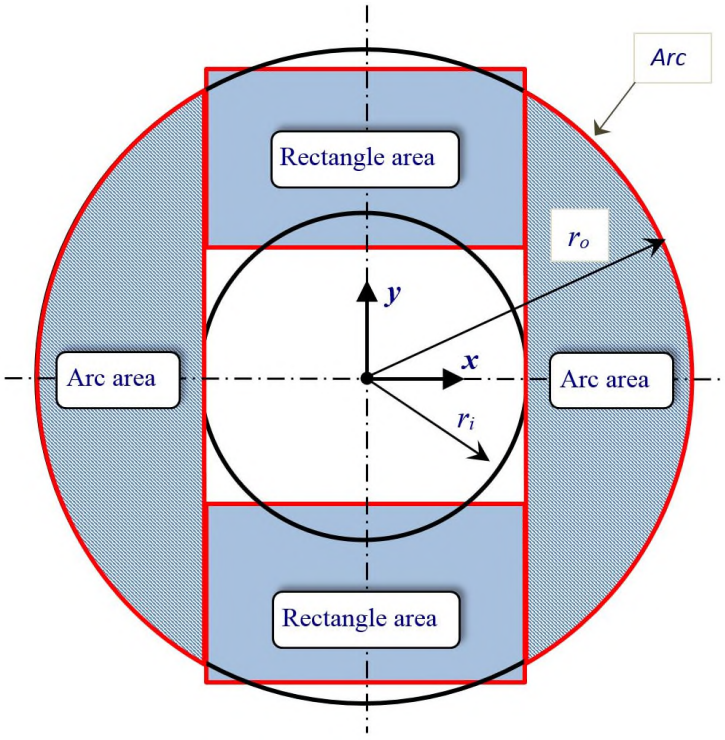

Figure 3: Partition of the disc friction surfaces into simplified geometry areas (not to scale)

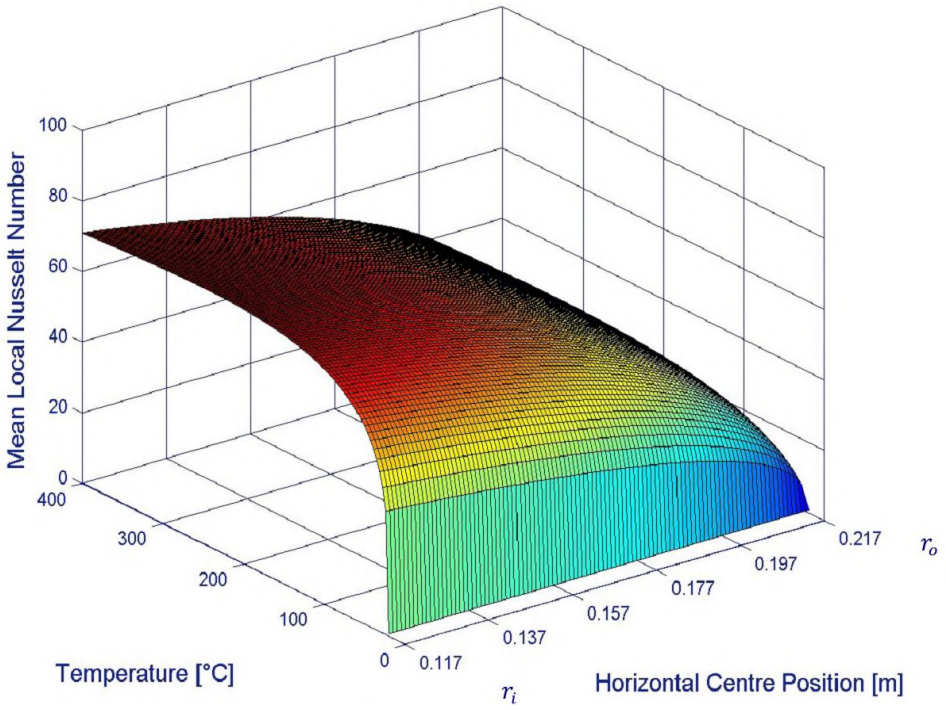

Figure 4: Mean Nusselt number for temperature and horizontal position, calculated for Churchill and Chu [12] relationship

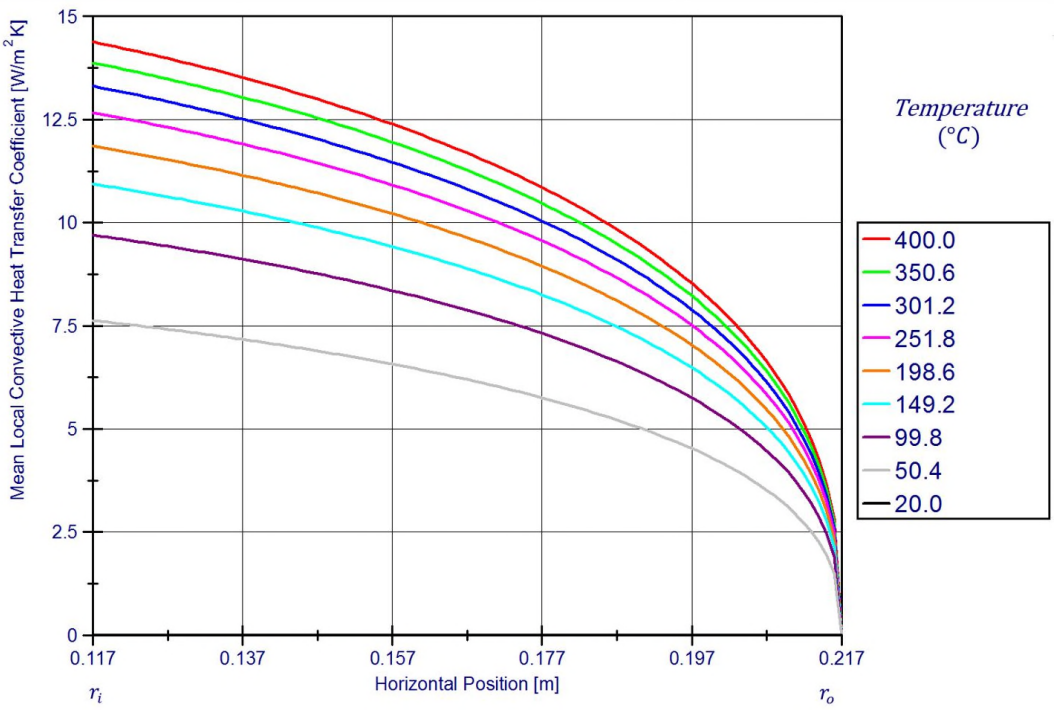

Figure 5: Calculated h_{conv} values for the Arc area – as per McAdams [10]

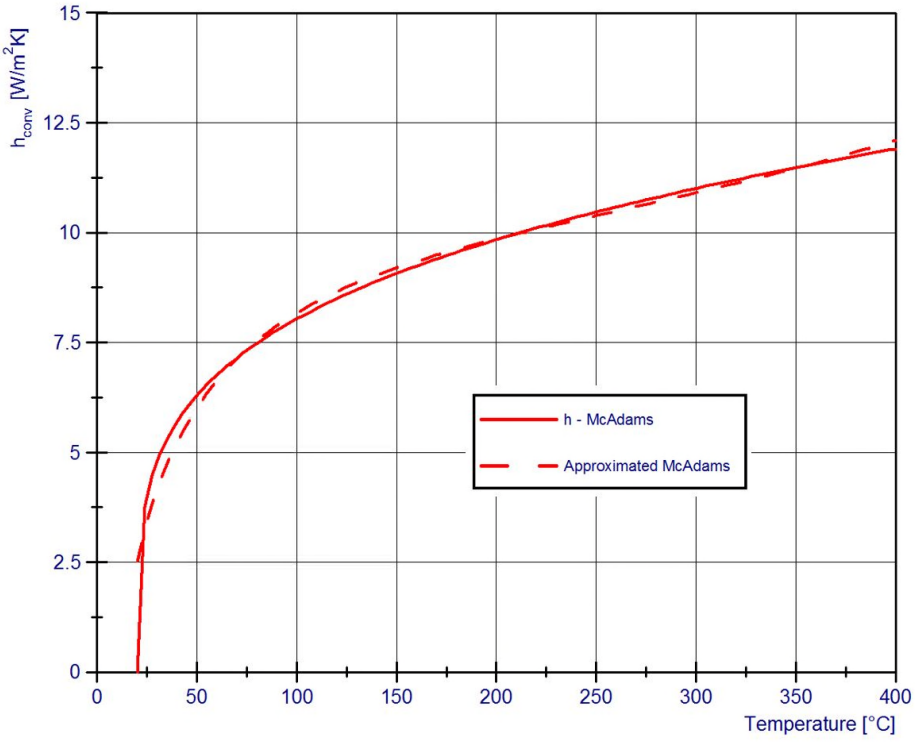

Figure 6: Mean h_{conv} values across the Arc area for various temperatures

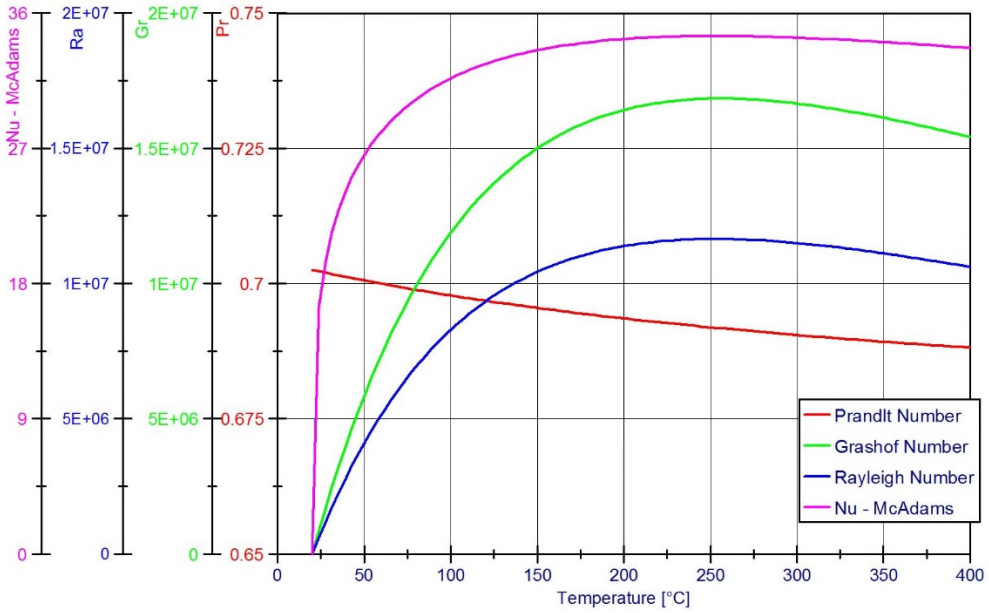

Figure 7: Calculated dimensionless parameters for the Rectangular area

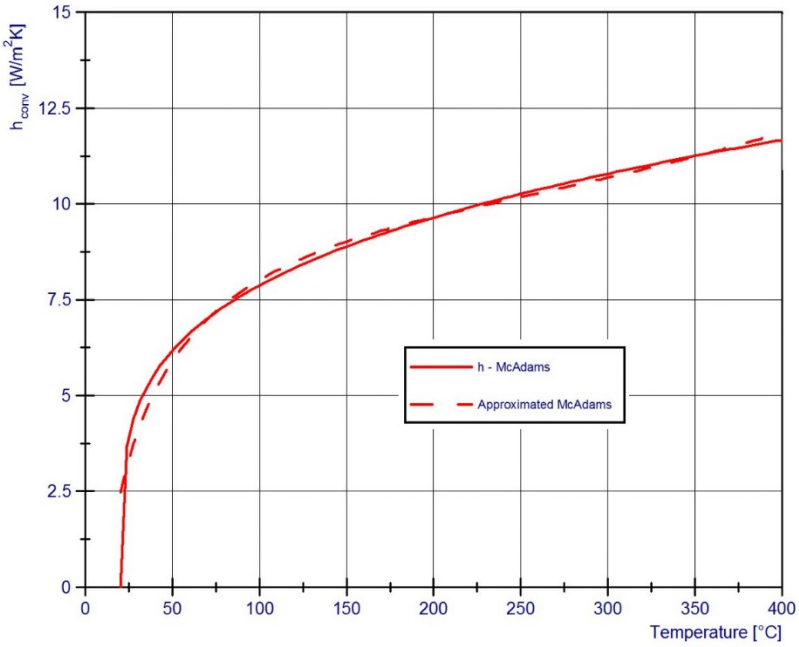

Figure 8: Mean h_{conv} values for the disc friction area

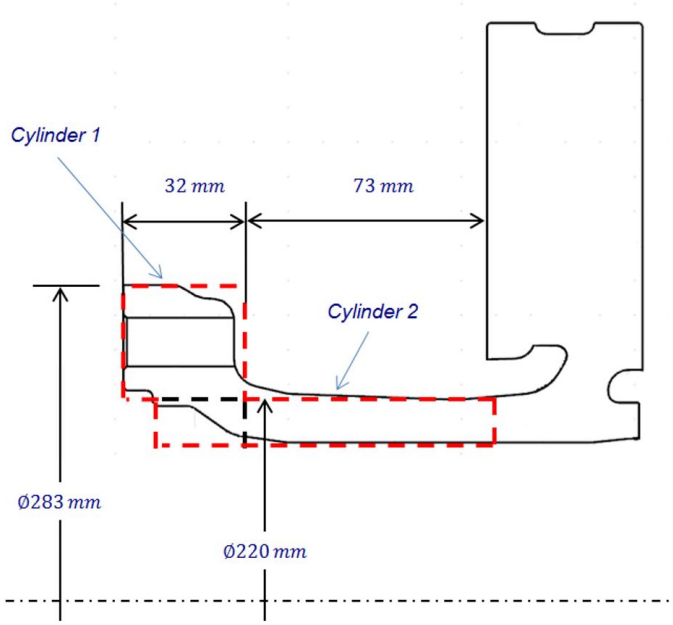

Figure 9: Simplified hat geometry

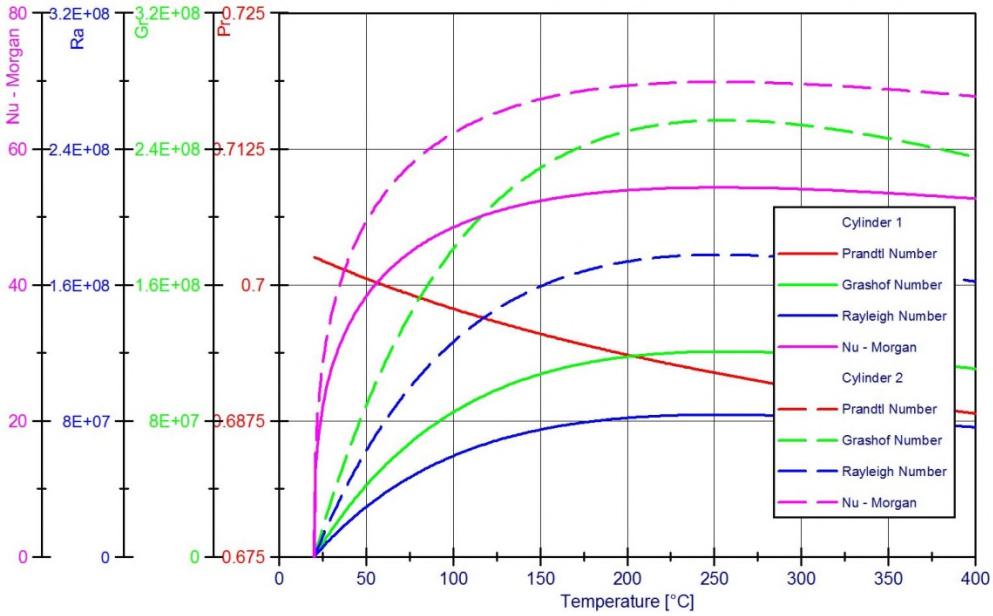

Figure 10: Dimensionless parameters for both cylinders representing hat geometry

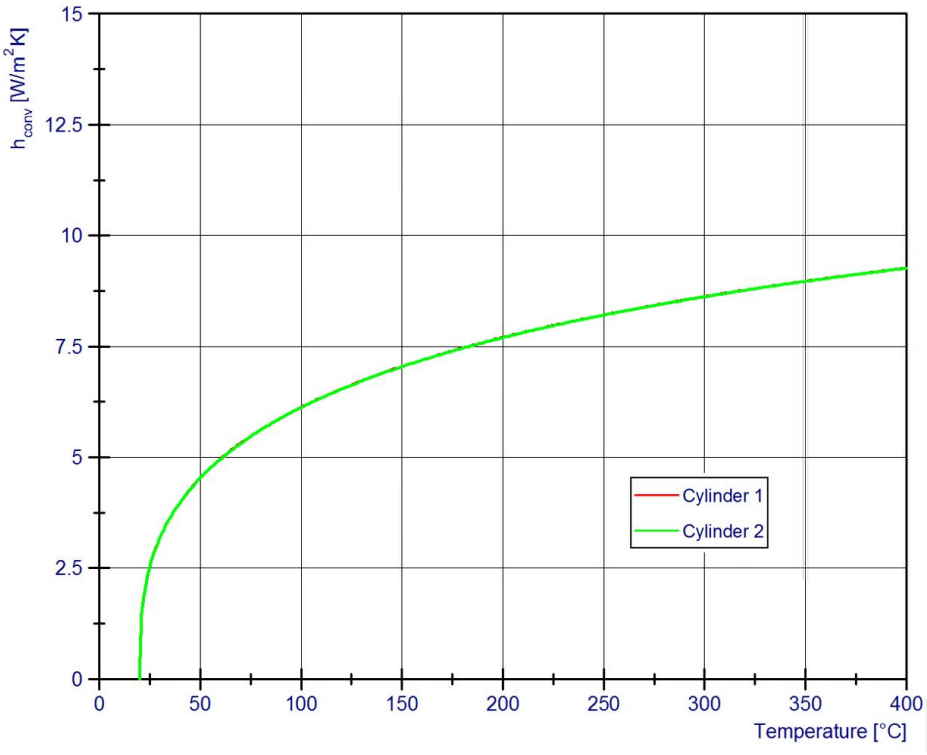

Figure 11: Mean h_{conv} values for the two cylinders (practically identical)

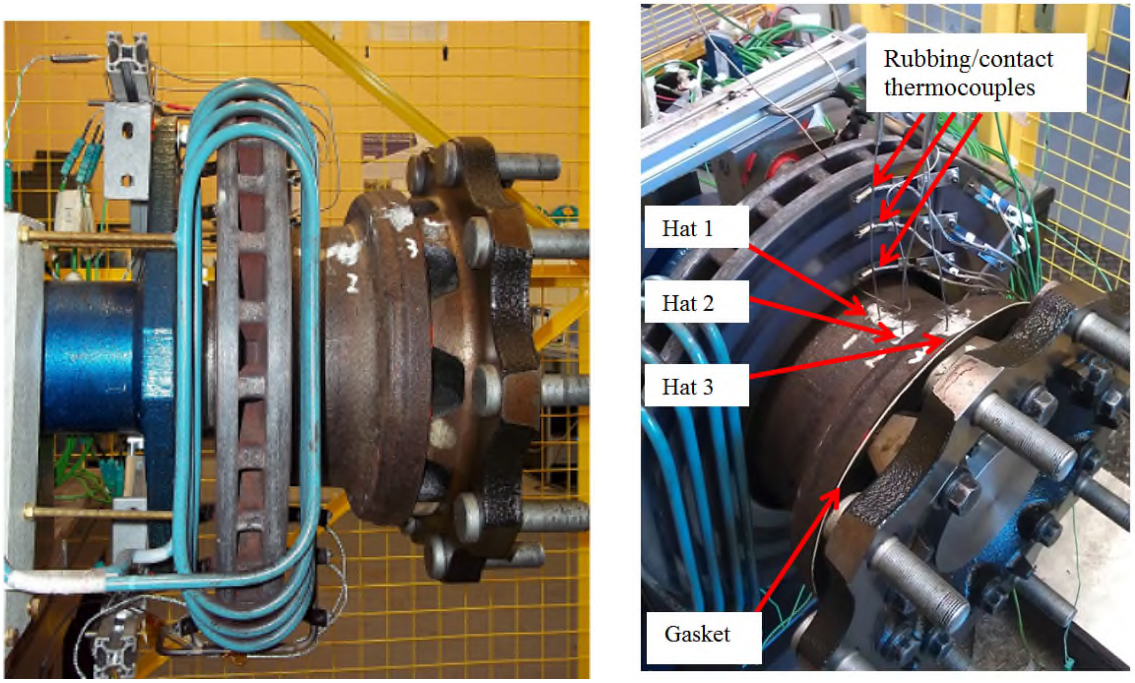

a) **b)**

Figure 12: Thermal Rig disc detail: a) Side view; b) The thermocouples

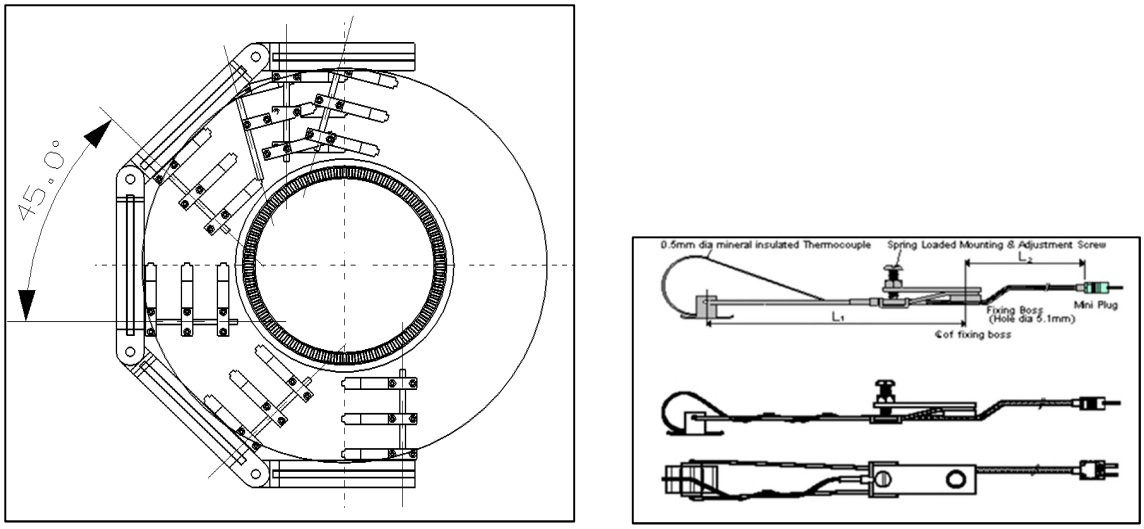

a) **b)**

Figure 13: Rubbing/contact thermocouples: a) Installation; b) Thermocouple detail

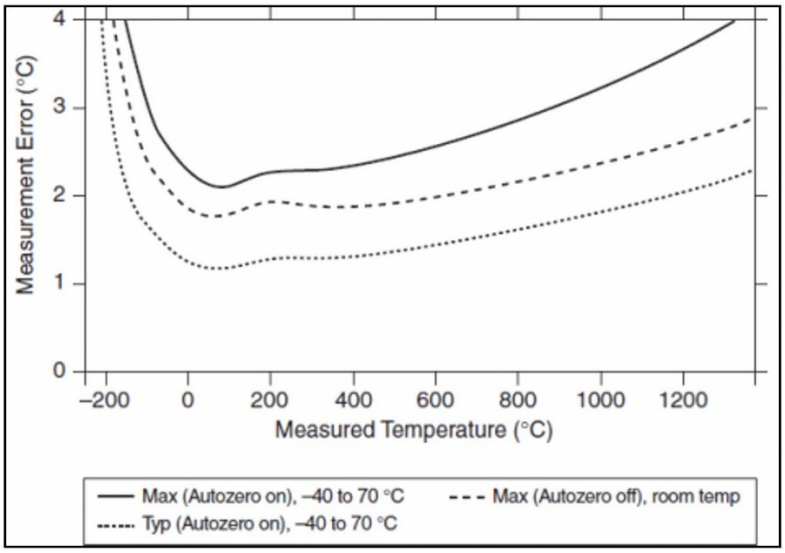

Figure 14: Thermocouple system error when using the NI 9211 module [16]

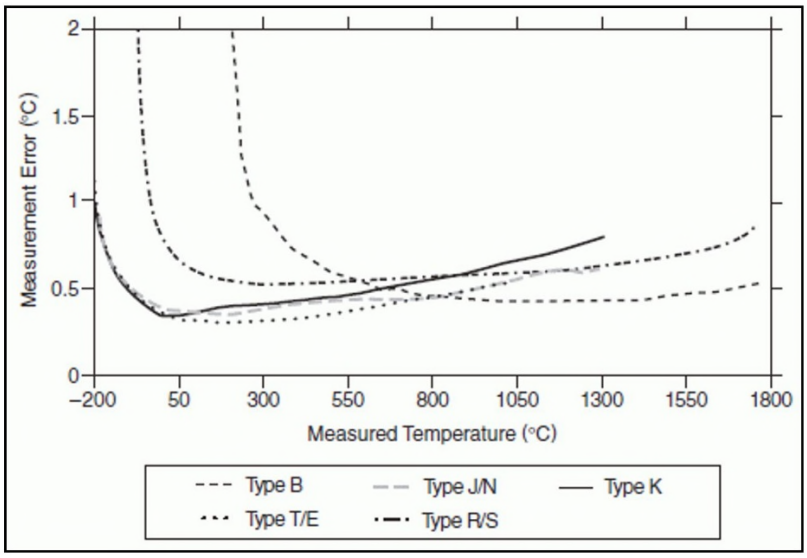

Figure 15: Thermocouple system error when using the NI 9214 module [16]

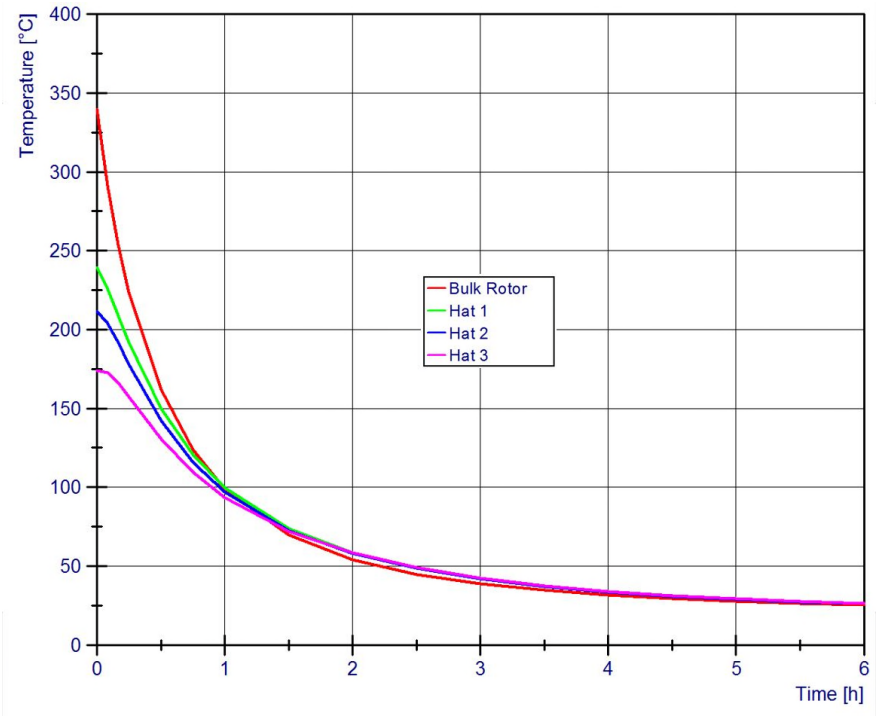

Figure 16: Disc rotor and hat temperatures taken from averaged experimental data

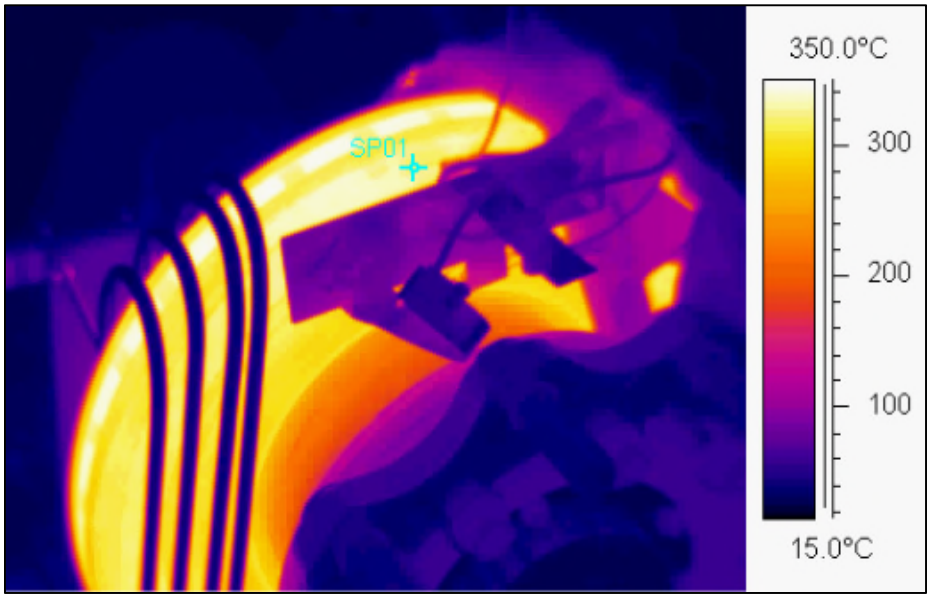

Figure 17: Thermal image of the initial parking application, showing the Spot temperature SP01 position and the adjacent +000 DOO thermocouple

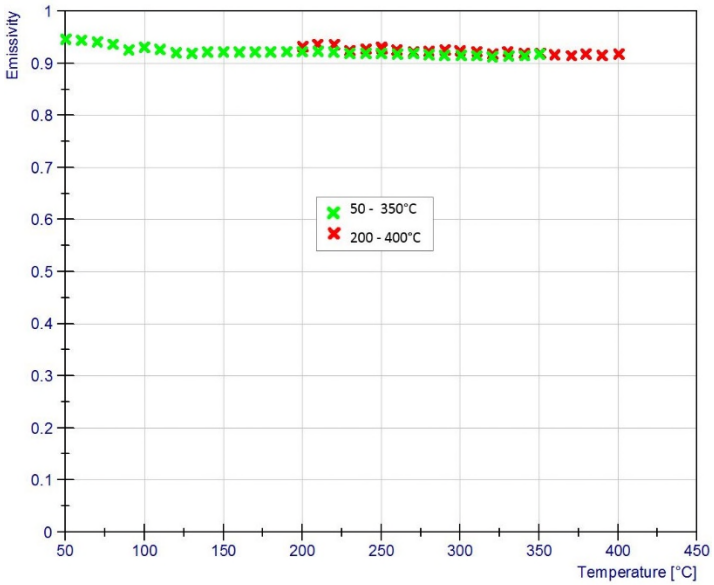

Figure 18: Emissivity results during the entire cooling phase

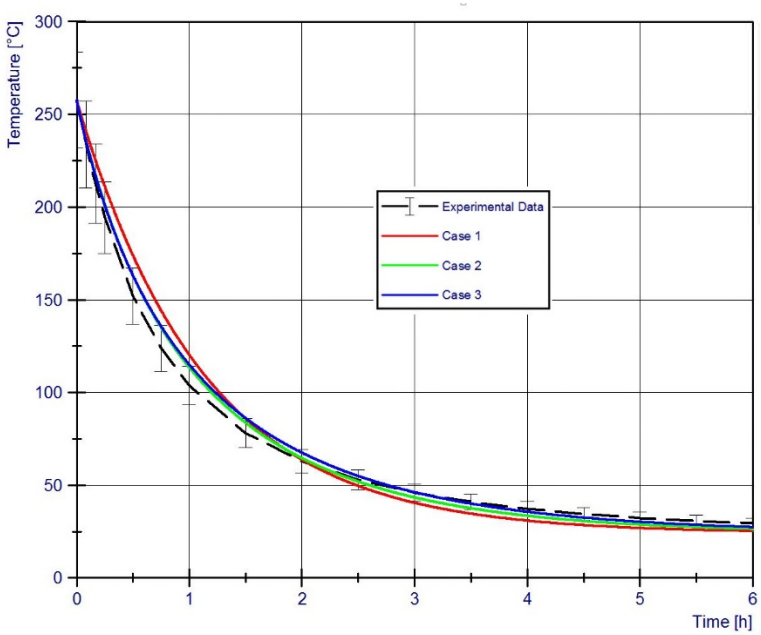

Figure 19: Comparison of the predicted (Cases 1, 2 and 3) and measured temperatures

2017-05-18

Heat dissipation from a stationary brake disc, Part 1: Analytical modelling and experimental investigations

Stevens, Kevin

SAGE

Kevin Stevens and Marko Tirovic. Heat dissipation from a stationary brake disc, Part 1: Analytical modelling and experimental investigations. Proceedings of the Institution of Mechanical Engineers, Part C: Journal of Mechanical Engineering Science, Vol. 232, Issue 9, 2018, pp. 1707-1733

http://dx.doi.org/10.1177/0954406217707983